SCIENTIFIC REPORTS
nature research

Check for updates

OPEN

A dynamic role for dopamine receptors in the control of mammalian spinal networks

Simon A. Sharples[1], Nicole E. Burma[2,3], Joanna Borowska-Fielding[4], Charlie H. T. Kwok[2,5], Shane E. A. Eaton[2,5], Glen B. Baker[6], Celine Jean-Xavier[5], Ying Zhang[4], Tuan Trang[2,5] & Patrick J. Whelan[2,5]✉

Dopamine is well known to regulate movement through the differential control of direct and indirect pathways in the striatum that express D_1 and D_2 receptors respectively. The spinal cord also expresses all dopamine receptors; however, how the specific receptors regulate spinal network output in mammals is poorly understood. We explore the receptor-specific mechanisms that underlie dopaminergic control of spinal network output of neonatal mice during changes in spinal network excitability. During spontaneous activity, which is a characteristic of developing spinal networks operating in a low excitability state, we found that dopamine is primarily inhibitory. We uncover an excitatory D_1-mediated effect of dopamine on motoneurons and network output that also involves co-activation with D_2 receptors. Critically, these excitatory actions require higher concentrations of dopamine; however, analysis of dopamine concentrations of neonates indicates that endogenous levels of spinal dopamine are low. Because endogenous levels of spinal dopamine are low, this excitatory dopaminergic pathway is likely physiologically-silent at this stage in development. In contrast, the inhibitory effect of dopamine, at low physiological concentrations is mediated by parallel activation of D_2, D_3, D_4 and α_2 receptors which is reproduced when endogenous dopamine levels are increased by blocking dopamine reuptake and metabolism. We provide evidence in support of dedicated spinal network components that are controlled by excitatory D_1 and inhibitory D_2 receptors that is reminiscent of the classic dopaminergic indirect and direct pathway within the striatum. These results indicate that network state is an important factor that dictates receptor-specific and therefore dose-dependent control of neuromodulators on spinal network output and advances our understanding of how neuromodulators regulate neural networks under dynamically changing excitability.

Neuromodulators are critical for central nervous system function and diversify circuit outputs by altering synaptic and intrinsic properties[1–3]. Dopamine is a monoamine neuromodulator that is well known for action selection in vertebrates through the control of direct and indirect circuits of the basal ganglia that express excitatory D_1 and inhibitory D_2 receptors respectively (for review, see Refs.[4–7] for examples). Dopamine is also important for the regulation of spinal motor networks that control rhythmic movements including but not limited to locomotion (for review, see Ref.[8]). In larval zebrafish, phasic and tonic firing patterns of descending neurons that provide the primary source of spinal dopamine correlates with locomotor episodes and quiescence, respectively[9]. These different firing patterns can impact the cellular release of dopamine and as a consequence, the receptor subtypes it activates[10]. For example, high levels of dopamine released during phasic cell firing activate lower affinity excitatory D_1 receptors and promote locomotor activity, and lower levels of dopamine released during tonic activity activate higher affinity inhibitory D_2 receptors and suppress motor output[11]. Similarly, dopamine has dose-dependent effects on locomotor circuits in precocial species with functional swim networks[12].

[1]School of Psychology and Neuroscience, University of St Andrews, Fife KY16 9JP, UK. [2]Hotchkiss Brain Institute, University of Calgary, HMRB 168, 3330 Hospital Drive NW, Calgary, AB T2N 4N1, Canada. [3]Department of Neuroscience, University of Calgary, Calgary, AB T2N 4N1, Canada. [4]Department of Medical Neuroscience, Dalhousie University, Halifax, NS B3H 4R2, Canada. [5]Department of Comparative Biology and Experimental Medicine, University of Calgary, Calgary, AB T2N 4N1, Canada. [6]Department of Psychiatry (NRU), Faculty of Medicine and Dentistry, University of Alberta, Edmonton, AB T6G 2G3, Canada. ✉email: whelan@ucalgary.ca

Figure 1. Dopamine evokes bidirectional dose-dependent modulation of lumbar network activity. (**A**) Extracellular neurograms recorded from naïve single lumbar ventral root preparations after applying dopamine in various concentrations. Each row indicates a separate trial. Each recording began with spontaneous motor activity; the green section shows the effect of dopamine for each dose. The red-dashed box highlights expanded sections of data to the right of each neurogram. (**B**) Mean normalized response ratios calculated from the root mean square of the raw neurogram during a 5-min window, 20 min after dopamine application, compared to baseline activity. The negative response ratios represent inhibition and positive values represent excitation. The number in each green bar indicates the number of preparations in the average for each concentration. Error bars indicate standard deviation. Asterisks denote the significance level of Tukey post hoc tests between ratio concentrations (*$p<0.05$, **$p<0.01$, ***$p<0.001$).

We have recently demonstrated that neuromodulation of developing mammalian spinal circuits is state-dependent[13] which is consistent with work in invertebrates[14,15]. This is important in developing spinal motor networks which produce a wide repertoire of patterned outputs at birth, including locomotor activity, as a consequence of dynamically fluctuating network excitability. That being said, neonatal rodents rarely produce coordinated bouts of locomotion and in vitro preparations of isolated spinal cord require pharmacological or electrical stimulation to drive the network into a high excitability state to produce fictive walking patterns. Instead, most of the movements observed in neonatal mice are ataxic. These movements correlate with spontaneous network activity, which can be observed in vitro[16–19]. Nevertheless, the vast majority of what we know about neuromodulation of developing mammalian spinal networks has been derived from studies on fictive locomotor activities with dopamine being predominantly excitatory when spinal networks are operating in this state[20–31].

mRNA for all 5 dopamine receptor subtypes is expressed in the mouse spinal cord and putative motoneurons by postnatal day 14[32] with similar mRNA distribution as early as day 4 (Allen Mouse Spinal Cord Atlas). However, prior to this time data on dopamine receptor expression is sparse. Changes in intrinsic properties and receptor expression can therefore lead to robust changes in neuromodulatory control of spinal circuits (Reviewed by Refs.[33,34]). Based on our previous work, we hypothesized that receptor actions, and therefore concentration-dependent control of network output by dopamine, is linked to the underlying network excitability state[13]. As a result, more complex receptor-dependent actions may have been masked during high excitability states of fictive locomotion. We therefore examined how dopamine modulates spinal output at the network and cellular level of neonatal mouse spinal cords in vitro during a low excitability state characterized by spontaneous activity[16,17]. Portions of these data were presented in abstract and preprint form[35,36].

Results

Dopaminergic modulation of spinal motor networks is dose-dependent and bidirectional. We focused on the modulation of perinatal spontaneous activity patterns to investigate how dopamine modulates spinal network output during a physiologically relevant low excitability state. Using the same experimental set-up as Sharples et al.[31], we recorded spontaneous motor activity with extracellular suction electrodes from single ventral roots of the second or fifth lumbar (L2/L5) segments simultaneously from two or four spinal cord preparations sharing the same chamber. Each preparation in these series of experiments was naïve to dopamine exposure and received only a single dose of its respective concentration. This configuration ensured consistent experimental conditions across several preparations exposed to different concentrations of dopamine. Low concentrations of dopamine (1–30 μM) consistently suppressed spontaneous motor activity, whereas higher concentrations (100–300 μM) excited spontaneous motor activity, evoking episodic and continuous rhythmic patterns (Fig. 1; $n=42$, $F_{(5,36)}=10.5$. $p<0.001$). A detailed description of the rhythmic activities generated by higher concentrations of dopamine 30–300 μM were analyzed using spectral analyses on data obtained from preparations included in this study and have been previously published[13].

Parallel actions of D_2, D_3, D_4, dopamine and alpha-2 adrenergic receptors mediate dopaminergic inhibition of spontaneous activity. To delineate receptor contributions to dopamine's bidirectional effects on endogenous spontaneous activity in isolated spinal cord preparations, we used antagonists selective for the family of dopamine receptors. At low concentrations of dopamine, we observed a negative response ratio (Fig. 2A,D1), which was due to a reduction in the number (Fig. 2D2), but not the amplitude, of spontaneous episodes (Fig. 2D3). In contrast to our hypotheses, the inhibitory effect of dopamine at low concentrations (10 μM) was not altered by antagonists targeting D_2 (L-741626; $n=3$, response ratio $=-0.57\pm0.26$), D_2/D_3 (sulpiride; 20 μM; $n=10$, response ratio $=-0.36\pm0.2$), D_3 (SB-27701-A, 5 μM; $n=3$; response ratio $=-0.36\pm0.3$), D_4 (L-745870; $n=3$, response ratio $=-0.32\pm0.1$) or D_1/D_5 receptors (Fig. 2B; SCH 23390; $n=4$, response ratio $=-0.43\pm0.2$). However, when all D_2-like receptors were blocked with a cocktail of sulpiride (D_2/D_3, 20 μM) and L-745870 (D_4, 5 μM), response ratios indicated that the inhibitory effect of 10 μM dopamine was attenuated, compared with dopamine alone (Fig. 2C; $n=6$; one-way analysis of variance (ANOVA), $F_{(4,32)}=7.3$, $p<0.001$; Tukey post hoc $p=0.09$), to a level where it was not significantly different from a time-matched vehicle control (Fig. 2C,D1; $n=6$, $F_{(4,32)}=7.3$, $p<0.001$; Tukey post hoc, $p=0.98$). Burst analysis revealed no difference in the number or amplitude of episodes when antagonists were present, compared with baseline (Fig. 2D2,D3; two-way ANOVAs for number, $F_{(2,28)}=9.5$, $p<0.0001$; two-way ANOVA for amplitude: $F_{(4,28)}=3.4$, $p=0.023$). Together these data suggest that the inhibitory actions of dopamine depend on parallel action of D_2, D_3 and D_4 receptors.

We considered the possibility that the inhibitory influence of low dopamine concentrations was partly due to the activation of non-dopamine receptors. Previous work conducted in our laboratory showed that dopamine inhibits cauda equina-evoked locomotion, partially via α_2-adrenergic receptors[28]. The remaining minor

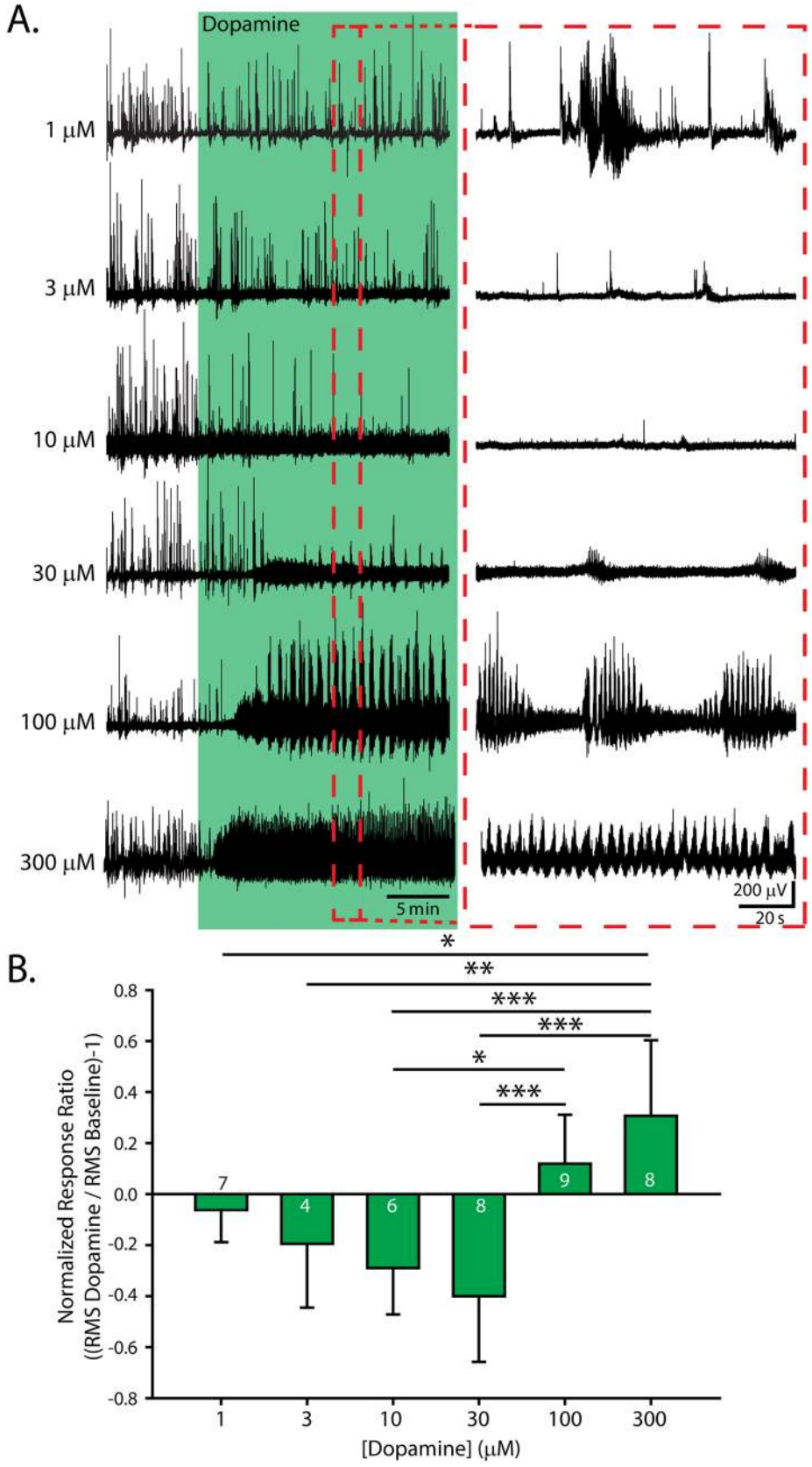
A.
Dopamine
1 μM
3 μM
10 μM
30 μM
100 μM
300 μM
5 min
200 μV
20 s
B.
Normalized Response Ratio
((RMS Dopamine / RMS Baseline)-1)
0.8
0.6
0.4
0.2
0.0
-0.2
-0.4
-0.6
-0.8
*
**
***
***
*
***
7
4
6
8
9
8
1
3
10
30
100
300
[Dopamine] (μM)

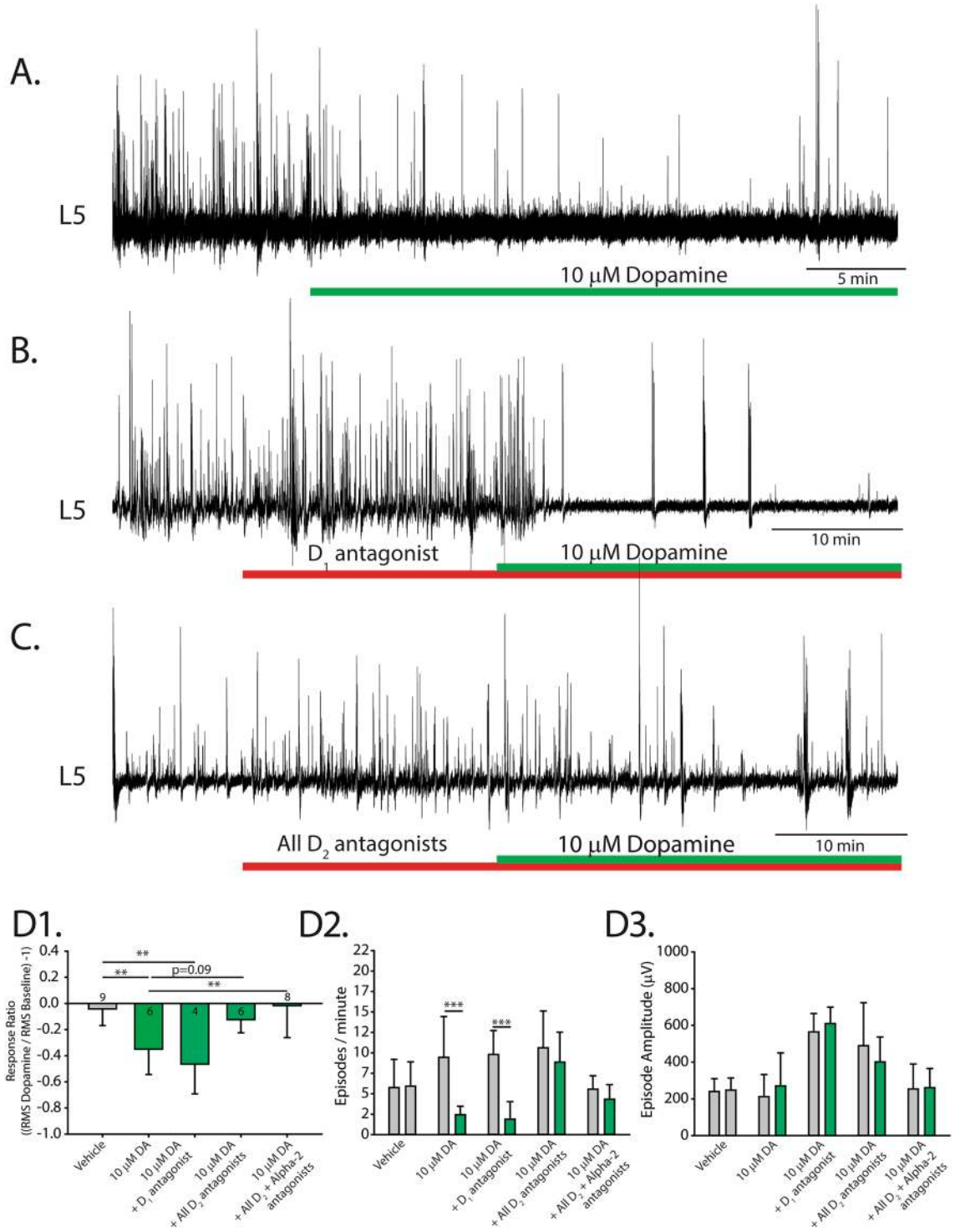

Figure 2. Receptor mechanisms for dopaminergic inhibition of spontaneous network activity. (**A**–**C**) Single ventral root (L5) extracellular neurograms of spontaneous activity in the presence of dopamine (**A**), a D_1 antagonist and dopamine (**B**), and with a cocktail of D_2 antagonists and dopamine (**C**). Spinal cords were perfused with receptor-preferring antagonists (red bars) 20 min prior to the application of low concentrations of dopamine (10 μM). (**D1**) Response ratio represents the root mean square of raw neurograms during a 5-min window, 20 min after dopamine application, compared with prior to dopamine application. Negative response ratios indicate inhibition and positive values indicate excitation. The number in each bar indicates the number of preparations included in that condition's mean. Bars indicate the mean (± SD), number of episodes per minute (**D2**), and amplitude (**D3**) of spontaneous episodes recorded within the 5-min epochs during which response ratios were calculated. Asterisks indicate the significance level of post hoc comparisons (*$p < 0.05$, **$p < 0.01$, ***$p < 0.001$).

inhibitory effect of dopamine at 10 μM was blocked by antagonizing the α_2-adrenergic receptors with yohimbine (4 μM) in the presence of D_2/D_3 and D_4 receptor antagonists. We observed significantly different response ratios, compared with 10 μM dopamine alone (Fig. 2D1; n = 6, $F_{(4,32)} = 7.3$, $p < 0.001$; Tukey post hoc, $p = 0.006$). Low dopamine concentrations did not change the number or amplitude of episodes in the presence of these antagonists, compared with baseline (Fig. 2D2,D3) suggesting that non-dopamine receptors also contribute to dopamine's inhibitory effects.

D_1–D_2 receptor coactivation contributes to dopaminergic excitation of spinal network activity. Dopamine binding to D_1 and D_2 heteromers can lead to depolarization via an increase in intracellular calcium levels, mediated by the enzyme phospholipase C (PLC)[37–40]. Thus, we first tested the role of the lower affinity D_1 receptor system and then examined whether the D_2 receptor system has a cooperative role in the control of spontaneous activity. With the addition of dopamine at higher concentrations (i.e., 50 and 100 μM), spontaneous activity patterns became rhythmic, often producing a slow rhythm with episodes of high frequency rhythmic activity. Moreover, the presence of the D_1-like receptor antagonist, SCH-23390, reduced this effect (Fig. 3; 100 μM dopamine with 10 μM SCH-23390; n = 5; response ratio, $F_{(5,35)} = 11.4$, $p < 0.001$); fast rhythm power, $F_{(4,27)} = 12.6$, $p < 0.001$; slow rhythm power, $H_{(4)} = 12.8$, $p = 0.013$; Fig. 3B,C, 50 μM dopamine with 10 μM SCH-23390; response ratio, $F_{(5,35)} = 11.4$, $p < 0.001$; fast rhythm power, $F_{(4,27)} = 12.6$, $p < 0.001$; slow rhythm power, $H_{(4)} = 12.8$, $p = 0.013$, Dunn's post hoc: $p = 0.03$; one way ANOVA used in tests). These results suggest that the excitatory effects of dopamine are primarily mediated by the D_1-like receptor family.

D_2 receptors have been previously reported to interact with D_1 receptors leading to excitatory responses[38–40]. We tested this idea by administering D_2-like antagonists (sulpiride + L745870) and found that the power of the fast rhythm elicited by dopamine at 100 μM was reduced (Fig. 3A3,B3,C2; n = 4; $F_{(4,27)} = 12.6$, $p < 0.001$) to the same extent as the D_1-antagonist, with no effect on the power of the slow rhythm (Fig. 3C3; $H_{(4)} = 12.8$, $p = 0.013$; Dunn's post hoc, $p = 1.0$). This suggests that D_2 receptors may contribute to the excitatory effects of dopamine.

To explore the interaction and co-activation profile of D_1 and D_2 receptors in isolated neonatal spinal cords, we performed co-immunoprecipitation for D_1 and D_2 receptors and used agonists to activate both receptor subtypes. After immunoprecipitating D_2 receptors from neonatal spinal cord lysates, we used an antibody to probe for D_1 receptors. We detected D_1 receptor protein within the D_2 receptor immunoprecipitates (Fig. 4C3) and these bands were blocked when pre-incubated with an antigen-blocking peptide. Raw unprocessed images of blots can be found in Supp. Fig. 3. This result indicates that D_1 and D_2 receptors may interact in neonatal mouse spinal cords.

In support of this idea, co-application of the D_1 agonist SKF 81297 (50 μM) and the D_2 agonist quinpirole (50 μM) elicited a more robust depolarization of the ventral root DC potential, compared with 50 μM of the D_1 agonist alone (Fig. 4A,C1; D_1, n = 8; D_1/D_2, n = 8; one-way ANOVA $F_{(2,21)} = 5.2$, $p = 0.01$; Tukey post hoc: $p = 0.02$). We observed no difference in the amount of spontaneous network activity evoked with co-application of a D_2 agonist, compared with application of the D_1 agonist alone, as indicated by the response ratio (Fig. 4B1–B3, C2; one-way ANOVA, $F_{(3,29)} = 12.0$, $p < 0.001$; Tukey post hoc, $p = 0.5$). In contrast, lower concentrations of the same agonists (10 μM) produced no effects (n = 8 for each condition; DC potential, $t_{(6)} = 0.73$, $p = 0.24$; response ratio, $t_{(6)} = 0.9$, $p = 0.19$). Thus, consistent with previous reports for striatal neurons[40], we found a dose-dependent effect of dopamine agonists wherein co-applying high doses, but not low doses, of D_1 and D_2 receptor agonists, produced more robust depolarization than a D_1 agonist alone.

In addition to co-applying separate D_1 and D_2 agonists, we tested co-activating D_1 and D_2-like receptors with the D_1/D_2 co-agonist SKF 83959 (50 μM)[39,41]. As predicted, the co-agonist elicited a more robust depolarization of the ventral root DC potential, compared with the D_1 agonist, when applied alone (Fig. 4A,C1; D_1 agonist, n = 8; D_1/D_2 agonist, n = 8; one-way ANOVA, $F_{(2,21)} = 5.2$, $p = 0.01$; Tukey post hoc, $p = 0.03$). Interestingly, the co-agonist also robustly facilitated superimposed spontaneous activity, as indicated by a larger response ratio than co-application of the D_1 and D_2 agonists produced (Fig. 4B,C2; one-way ANOVA, $F_{(3,29)} = 12.0$, $p < 0.001$; Tukey post hoc, $p = 0.004$). These data suggest that under certain conditions, D_2 receptors that are typically inhibitory can play an excitatory role and may interact with D_1 receptors to contribute to lumbar motor network excitation in the neonatal mouse spinal cord.

Low levels of endogenous spinal dopamine inhibit spontaneous activity. We next examined how the endogenous dopamine system regulates perinatal spinal network function. Endogenous levels of dopamine were increased by blocking the dopamine transporter (DAT) with an antagonist GBR 12909 (10 μM). Blocking DAT (n = 8 preparations) produced a modest but significant reduction in spontaneous activity compared to time-matched vehicle controls, reflected by a reduced response ratio (Fig. 5A,B1; one-way ANOVA, $F_{(2,19)} = 18.0$, $p < 0.001$) and a reduced number of spontaneous episodes (Fig. 5B2; n = 8, two-way ANOVA, $F_{(2,20)} = 11.8$, $p = 0.0004$), with no change in amplitude (Fig. 5B3; n = 6, two-way ANOVA, $F_{(2,20)} = 1.3$, $p = 0.3$). We questioned whether extracellular dopamine metabolism may have dampened the effect of the reuptake blocker, thus diminishing the predicted increase in endogenous dopamine levels. Therefore, we repeated this experiment in the presence of bifemelane, a monoamine oxidase A and B inhibitor. Under these conditions, we found further reductions in spontaneous activity when DAT was blocked, as indicated by a significantly reduced response ratio (Fig. 5B1; n = 6, one-way ANOVA, $F_{(2,19)} = 18.0$, $p < 0.001$). Burst analysis revealed significantly fewer episodes (Fig. 5B2; n = 6, two-way ANOVA, $F_{(2,20)} = 11.8$, $p = 0.0004$) with no change in amplitude (Fig. 5B3; n = 6, two-way ANOVA, $F_{(2,20)} = 1.3$, $p = 0.3$).

We followed these experiments up with high-performance liquid chromatography (HPLC) to verify endogenous levels of dopamine. In P3 lumbar spinal cords (n = 11) we detected low levels of dopamine; in P60 adults (n = 17) we detected a threefold increase in dopamine levels compared to at P3 (Fig. 5B4; Mann–Whitney

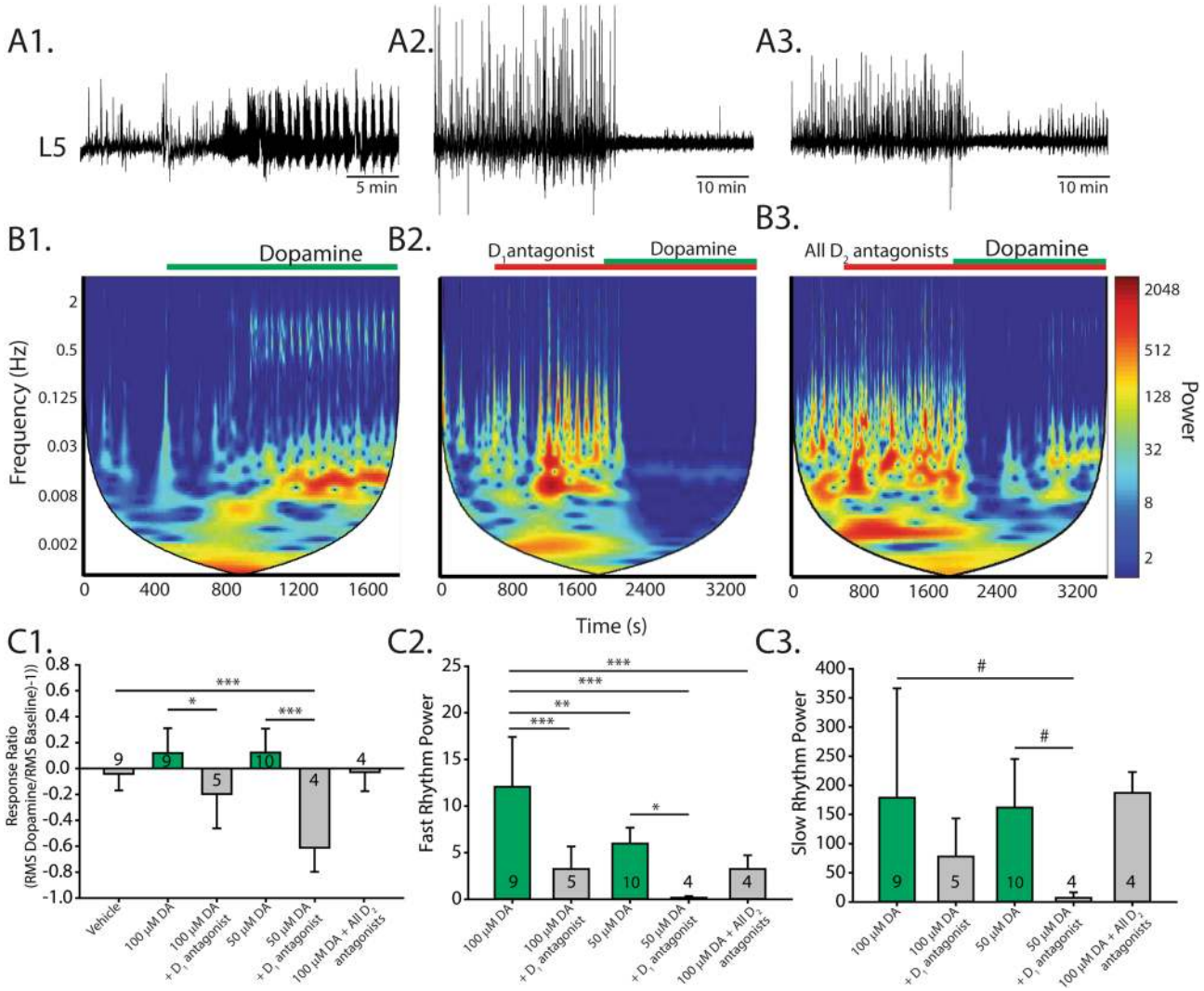

Figure 3. Receptor mechanisms for dopaminergic excitation of spinal network activity. High concentrations of dopamine excite spinal networks and produce episodic and continuous rhythmic patterns of activity. (**A**) Single ventral root extracellular neurograms of spinal network activity from each condition: dopamine applied alone (**A1**), in the presence of a D_1 antagonist (**A2**), and with a cocktail of D_2 antagonists (**A3**). Horizontal bars indicate the timing of dopamine application (green bars) and the application of receptor-preferring antagonists (red bars). (**B**) Spectrograms show autowavelet frequency power across time, evoked at high concentrations of dopamine (50–100 µM). The colour bar indicates power magnitude, from high (warm) to low (cool colours). We selected regions of interest around regions that coincided with fast and slow rhythm frequency rhythms. Spinal cords were perfused with antagonists for 20 min prior to the application of dopamine. (**C1**) Mean response ratios (± SD), as in Fig. 2, for each condition. Spectral analysis of fast rhythm (**C2**) and slow rhythm (**C3**) power following drug application for each experimental condition. Histograms present mean values ± SD, with asterisks denoting significance level of post hoc tests (*$p < 0.05$, **$p < 0.01$, ***$p < 0.001$) following one-way ANOVA (fast rhythm; **C2**) or nonparametric one-way ANOVA (slow rhythm; **C3**).

$U = 10.0$, $T = 76$, $p < 0.001$). Thus, our in vitro experiments indicated that low levels of endogenous dopamine play a role in D_2-mediated inhibition.

D_1 receptor activation increases motoneuron excitability by reducing afterhyperpolarization properties. In the next set of experiments, we were interested in determining the cellular mechanisms that mediate dopamine's complex modulatory effects on spinal network output. As integrators of premotor network activity that generate many of the rhythmic outputs of the spinal cord, motoneurons are ideally suited to amplify spontaneous activity and respond to dopaminergic modulation. Given that they not only serve as the final output for spinal networks, but they also participate in the generation of rhythmic activity[42], we initially selected motoneurons as a locus for determining the cellular mechanisms for dopaminergic excitation and inhibition. We made whole-cell patch-clamp recordings from 75 motoneurons (across 42 animals: mean ± SD age: 2.4 ± 1.1 days old; Range P0–P4). Some of these motoneurons (n = 18 across seven animals) were filled

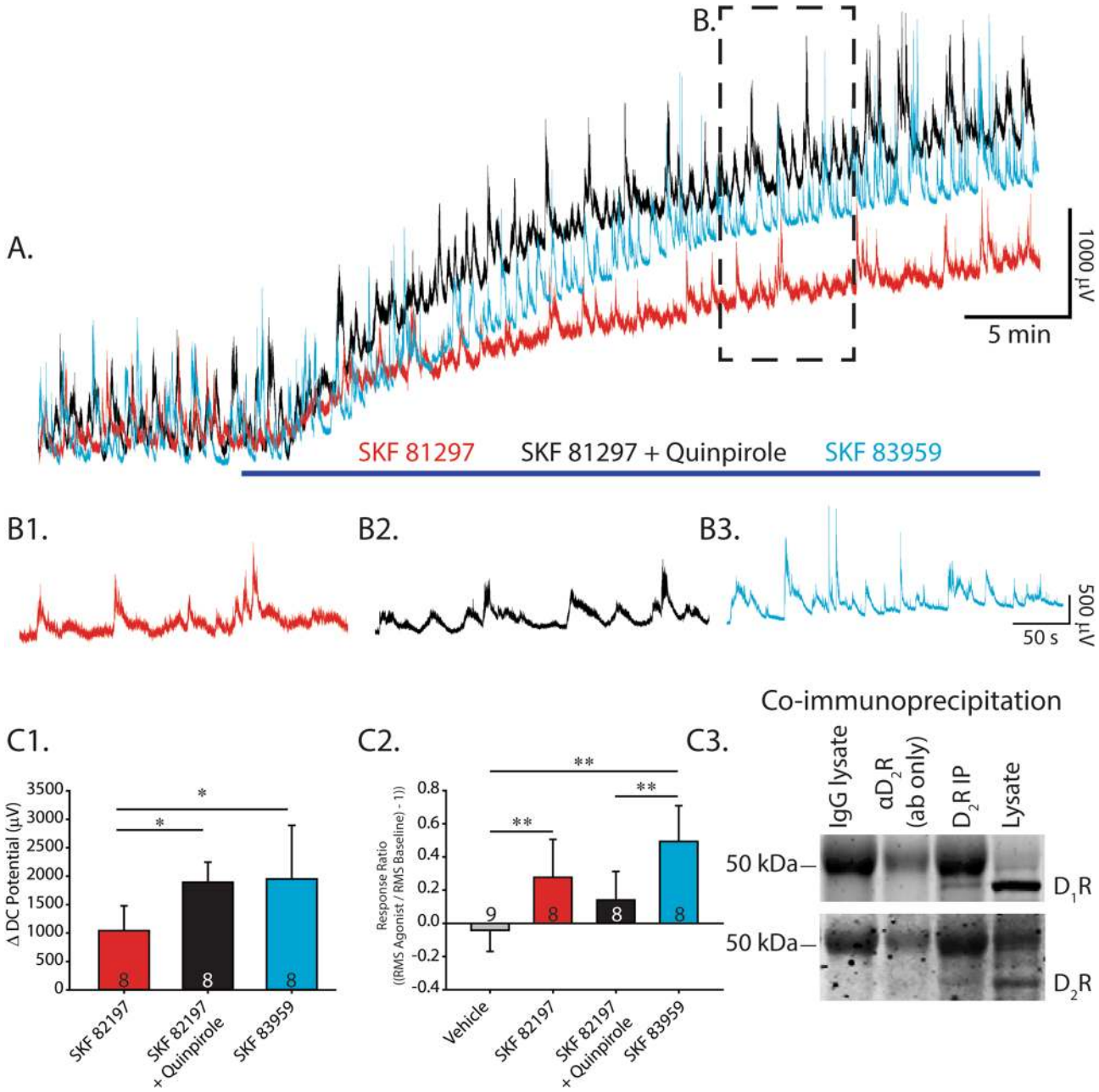

Figure 4. D_1 D_2 receptor co-activation contributes to the excitatory effect of dopamine. (**A**) Single ventral root extracellular DC neurograms of spontaneous activity from conditions where a D_1 agonist (SKF 81297) was applied alone (red), co-applied with a D_2 agonist (SKF 81297 + Quinpirole; black), or D_1 and D_2 receptors were coactivated by a D_1/D_2 co-agonist (SKF 83959; blue). The period of time when drugs were washed in is denoted by the navy-blue bar. B1-3. For each agonist, (**B**) expands the region of spontaneous activity 20–25 min after agonist application, as outlined by the dashed line in (**A**). (**C**) **C1** Depicts depolarization of DC potentials from DC neurograms, averaged across the number of preparations denoted by numbers in each condition's bar. **C2** Shows the response ratio for each condition (as in previous figures), which represents changes in the amount of spontaneous activity. (**C3**) Co-immunoprecipitation of D_1 with D_2 receptors suggests that they may interact in the neonatal spinal cord. Histograms present mean values ± SD, with asterisks denoting significance level of post hoc comparisons (*$p < 0.05$, **$p < 0.01$, ***$p < 0.001$) following one-way ANOVA.

with fluorescein-conjugated dextran amine (FITC; Molecular Probes, Inc., Eugene Oregon) and verified post hoc using immunohistochemistry for the presence of choline acetyltransferase (ChAT; Fig. 6A). One hundred percent of filled cells were ChAT positive indicating that we were indeed recording from motoneurons. Electrical properties measured in a group of these cells (n = 8 cells across five animals; Supp. Figure 2) were comparable to cells from putative motoneurons recorded in the subsequent experiments (Table 1) indicating that these cells are also likely motoneurons. Capacitance ($\mathbf{C_m}$: 200 ± 51 pF; Range 70–285 pF), input resistance ($\mathbf{R_{in}}$:

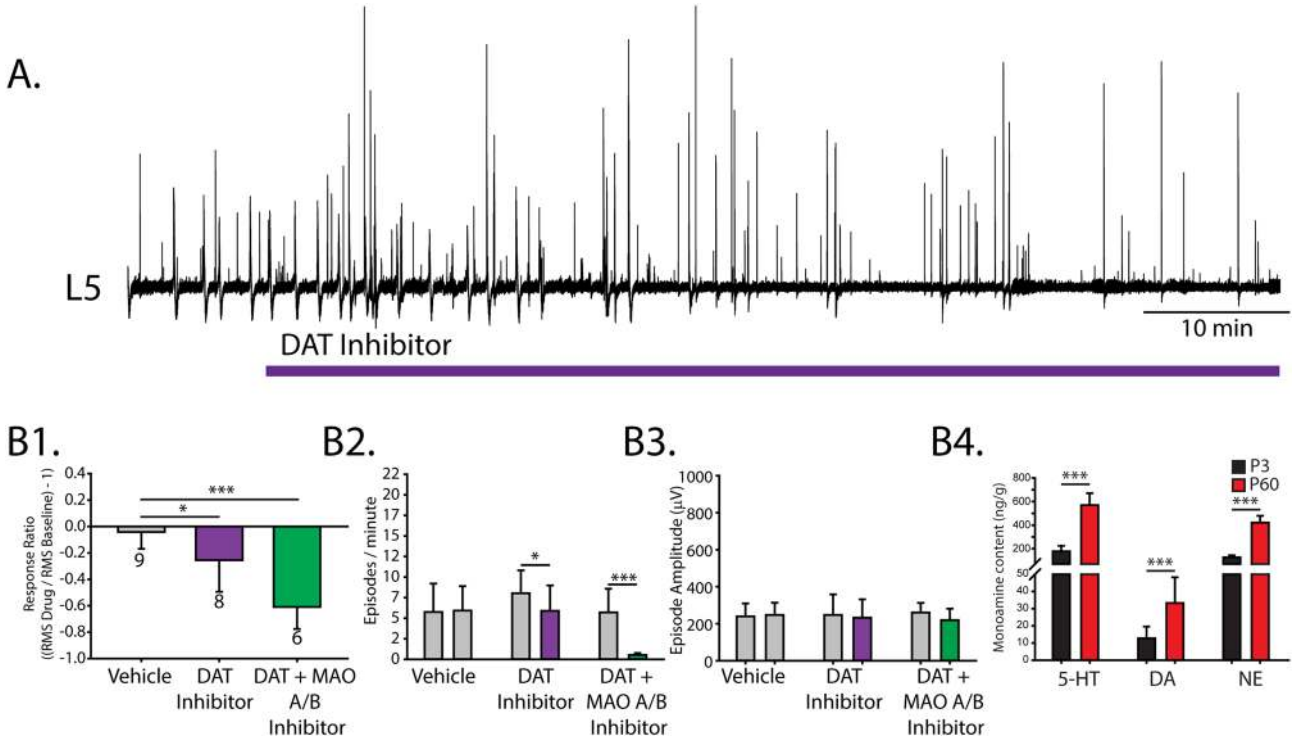

Figure 5. Inhibitory actions of endogenous dopamine in the neonatal mouse spinal cord. (**A**) Single ventral root (L5) neurogram of spontaneous activity after blocking the dopamine transporter (DAT) with the DAT antagonist GBR 12909 (purple) to increase the endogenous dopamine level. Dopamine reuptake was also blocked in the presence of monoamine oxidase (**A**, **B**) inhibitor bifemelane (green) to reduce dopamine metabolism. **B1** illustrates the response ratio; negative and positive values indicate inhibition and excitation, respectively. The number below each bar represents the number of preparations for each experiment. Spontaneous episode occurrences per minute (**B2**) and amplitude (**B3**) were measured within the epochs where the response ratio was calculated. Histograms present mean values ± SD and asterisks indicate a significance level of post hoc analyses (*$p < 0.05$, **$p < 0.01$, ***$p < 0.001$) following one-way ANOVA for response ratios, and two-way ANOVA for burst occurrences and amplitude that compared between conditions. (**B4**) Endogenous levels of serotonin (5-HT), dopamine (DA) and norepinephrine (NE) were measured in neonatal (P3) and adult (P60) lumbar spinal cords with high-performance liquid chromatography.

45 ± 34 MΩ; Range 25–180 MΩ), resting membrane potential ($\mathbf{V_m}$: −73 ± 4.9 mV; Range −81 to −61 mV) and bias current ($\mathbf{I_{hold\ -75}}$: −8.1 ± 93 pA; Range −160 to 180 pA) for the 75 motoneurons included in this study are equivalent to those reported in the literature[43–46]. Motoneurons recorded from animals age P3–4 days old had a significantly higher capacitance than those recorded from animals P0–2 days old (**P0–2**: n = 42; $C_m = 188 \pm 51$ pF; **P3–4**: n = 35; $C_m = 216 \pm 47$ pF; $t_{(75)} = 2.4$, $p = 0.02$); but did not differ in input resistance (**P0-2**: $R_{in} = 50 \pm 40$ MΩ,; **P3–4**: $R_{in} = 38 \pm 24$ MΩ; $t_{(56)} = 1.3$, $p = 0.2$). Motoneurons also display characteristic time-dependent changes in repetitive firing frequency during sustained depolarizing current injections[47–49]. We found that all but two cells demonstrated a time-dependent reduction in firing rate throughout the duration of a 0.5 s depolarizing current injection, as indicated by the ratio between maximum steady-state and first spike interval frequencies. This phenomenon is known as spike frequency adaptation (SFA; mean SFA ratio = 0.47 ± 0.19). In addition, doublet firing occurred at the onset of repetitive firing in 5 cells (8%).

Consistent with previous reports from our laboratory[50,51] and with our network recordings in this report, 100 μM of dopamine increased motoneuron excitability (n = 5 cells across four animals); we reproduced this effect with the D_1 agonist SKF 81297 (20 μM; n = 8 cells across five animals). Cells were held at -75 mV in voltage clamp (Fig. 6B1) while drugs were bath—applied onto slices and in current clamp for 2 cells while a high concentration of dopamine was washed on (Fig. 6B2). Both 100 μM dopamine and the D_1 agonist depolarized the membrane potential (Fig. 6C1; $H_{(2)} = 18.9$, $p < 0.001$), increased the amount of bias current required to maintain membrane potential at −75 mV (vehicle, −7.1 ± 33 pA; DA, −247 ± 78 pA; D_1, −174 ± 49 pA; $H_{(2)} = 18.9$, $p = 0.001$) increased the input resistance (Fig. 6C2; $H_{(2)} = 16.0$, $p < 0.001$), and decreased rheobase (Fig. 6C3; $F_{(2,22)} = 5.0$, $p = 0.016$) beyond that of the time-matched vehicle control. We found no change in spike rise time ($F_{(2,22)} = 1.0$, $p = 0.4$) or half width ($F_{(2,22)} = 0.8$, $p = 0.5$). The D_1 agonist reduced the amplitude of the afterhyperpolarization (AHP) to a greater extent than the time-matched vehicle control. 100 μM dopamine also reduced AHP amplitude compared to baseline, however, the change was not greater than that of the time-matched vehicle control (Fig. 6C4; $F_{(2,22)} = 7.7$, $p = 0.003$). Frequency–current (FI) relationships were measured during the first spike interval and steady-state firing in response to a series of depolarizing current pulses (Fig. 6D1,E1). Both 100 μM dopamine and the D_1 agonist reduced the latency to first spike beyond that of the time-matched vehicle control (Fig. 6F1;

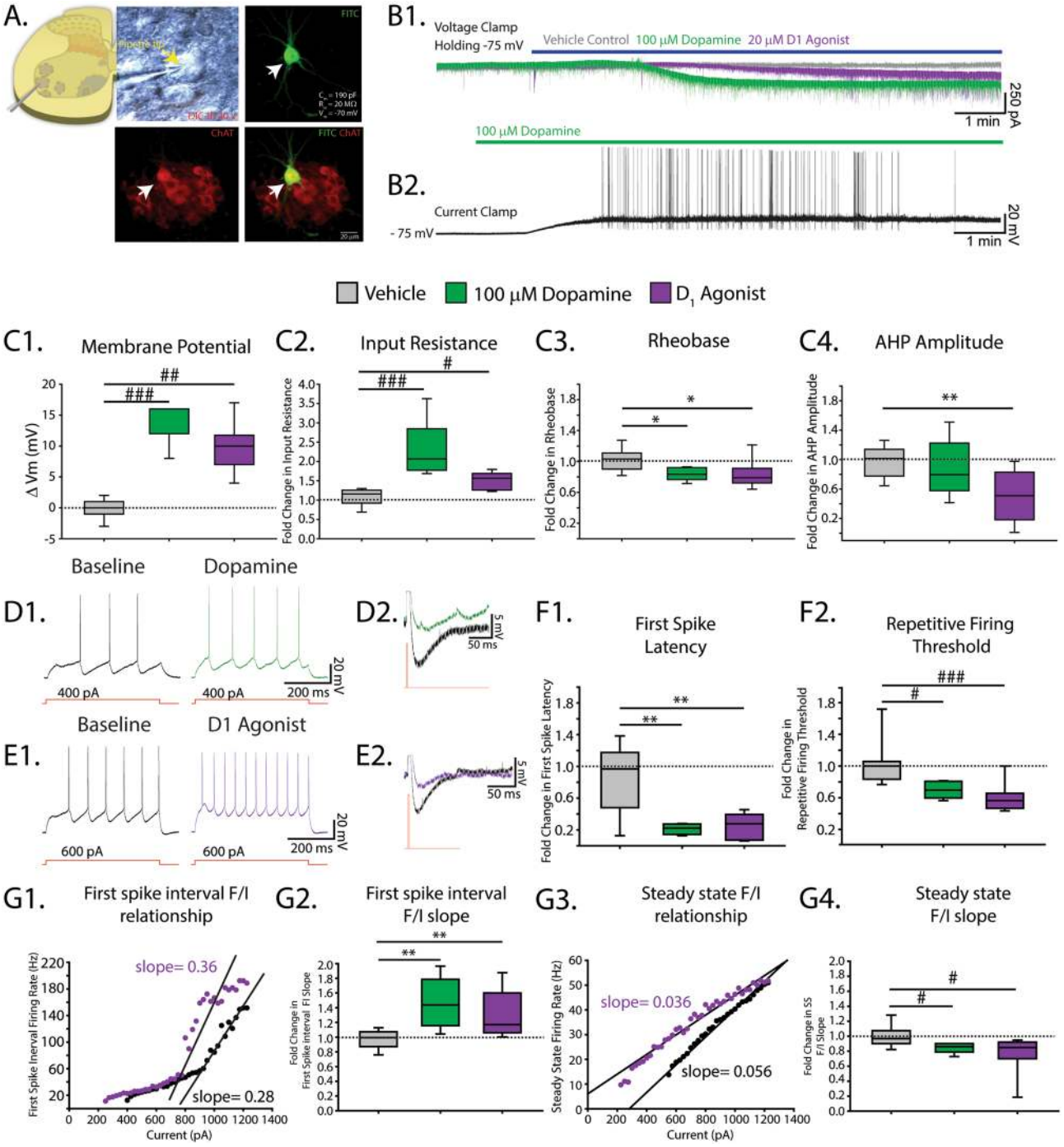

Figure 6. High concentrations of dopamine and D_1 agonists increase motoneuron excitability and reduce AHP properties. (**A**) Whole-cell patch-clamp recordings were obtained from motoneurons visualized with infrared differential interference contrast (IR-DIC) in lumbar slices of neonatal (P0–P4) mice. A subset of cells were filled with fluorescein (FITC, green) and verified post hoc with immunohistochemistry for choline acetyltransferase (ChAT, red). (**B1**) Representative voltage clamp traces from motoneurons exposed to a vehicle (H_2O; grey), high concentration of dopamine (100 µM, green) or the D_1 agonist SKF 81297 (20 µM, purple). (**B2**) Current clamp trace from a motoneuron exposed to a high concentration of dopamine (100 µM, green bar). (**C1**–**C4**) High concentrations of dopamine (100 µM, green) and the D_1 agonist SKF 81297 (20 µM, purple) depolarized the resting membrane potential (**C1**), increased input resistance (**C2**), decreased rheobase (**C3**) and AHP amplitude (**C4**.). (**D1**, **E1**) Representative current clamp traces of repetitive firing elicited by a 500 ms depolarizing current step and in (**D2**, **E2**) afterhyperpolarization before (black) and after high dopamine (green) or the D_1 agonist (purple). A high concentration of dopamine and the D_1 agonist reduced the latency to first spike measured during the first 500 ms current step (denoted repetitive firing threshold) and also reduced repetitive firing threshold (**F2**). **G1**, **G3** display a representative frequency–current (**FI**) plot for the first spike interval (**G1**) and steady state firing (**G3**) from a single cell before (black dots) and after (purple dots) application of the D_1 agonist. Fold change in first spike (**G2**) and steady state (**G4**) FI slopes. All measures were compared to that of time-matched vehicle control (grey) and displayed as fold change relative to their respective baseline values reported in Table 1. Box and whisker plots display interquartile range (boxes), median (horizontal black lines), max, and minimum value in data range (whiskers). Asterisks denote significance level of post hoc tests (*$p < 0.05$, **$p < 0.01$, ***$p < 0.001$) following one-way ANOVA.

Property	Chat⁺ filled MNs (8,5)	Vehicle[a] (12,6)	1 µM DA (7,4)	5 µM DA (7,4)	10 µM DA (6,5)	100 µM DA (5,4)	SKF 81,297 (8,5)	Quinpirole (12, 7)	(7,56) F, *p*
Motoneuron basal properties [N = 65 MNs, 40 animals (P0–P4)]									
Passive properties									
Capacitance (pF)	203 ± 54	203 ± 35	193 ± 55	194.3 ± 45	149 ± 66	244 ± 54	199 ± 50	210 ± 43	1.6, 0.15
V_m (mV)	−73 ± 4.1	−74 ± 4.3	−75 ± 4.1	−73 ± 4.7	−73 ± 3.7	−76 ± 3.5	−72 ± 6.1	−73 ± 5.0	0.7, 0.7
$I_{bias-75\ mV}$ (pA)	−86 ± 148	−25 ± 138	26 ± 125	−63 ± 85	23 ± 150	−101 ± 99	−38 ± 87	−74 ± 62	1.16, 0.3
Rin (MΩ)	50 ± 15	48 ± 24	59 ± 44	70 ± 83	115 ± 84	40 ± 9.2	71 ± 28	49 ± 14	2.0, 0.07
Rheobase (pA)	678 ± 225	747 ± 386	596 ± 367	464 ± 286	443 ± 390	762 ± 318	580 ± 298	633 ± 260	0.9, 0.5
Spike properties									
AP_{TH} (mV)	−51 ± 4.4	−55 ± 4.4	−55 ± 4.2	−52 ± 5.9	−56 ± 3.5	−53 ± 2.5	−54 ± 4.3	−55 ± 4.4	1.0, 0.4
AP_{AMP} (mV)	66 ± 5.0	71 ± 5.9	75 ± 6.9	76 ± 13	76 ± 4.2	69 ± 5.7	71 ± 9.6	72 ± 6.1	1.6, 0.2
$AP_{rise\ time}$ (ms)	0.45 ± 0.2	0.33 ± 0.1	0.37 ± 0.1	0.4 ± 0.1	0.44 ± 0.1	0.32 ± 0.04	0.35 ± 0.05	0.33 ± 0.1	1.6, 0.2
$AP_{half\ width}$ (ms)	0.59 ± 0.15	0.60 ± 0.1	0.64 ± 0.2	0.78 ± 0.3	0.75 ± 0.2	0.62 ± 0.07	0.68 ± 0.1	0.68 ± 0.19	1.2, 0.3
$AHP_{duration}$ (ms)	73.7 ± 29	70 ± 18	88 ± 34	76 ± 13	108 ± 38	74 ± 16	69 ± 23	76 ± 26	1.5, 0.2
AHP_{AMP} (mV)	−3.9 ± 1.1	3.6 ± 2.2	3.1 ± 1.4	3.2 ± 1.4	3.4 ± 2.1	4.7 ± 1.2	−4.2 ± 1.9	−4.3 ± 1.4	0.8, 0.6
Repetitive firing properties									
SS F/I Slope (Hz/pA)	0.053 ± 0.01	0.044 ± 0.008	0.058 ± 0.008	0.052 ± 0.018	0.053 ± 0.03	0.051 ± 0.007	0.046 ± 0.008	0.053 ± 0.012	1.2, 0.3
Repetitive firing TH (pA)	605 ± 446	498 ± 254	410 ± 271	354 ± 200	338 ± 327	515 ± 253	367 ± 186	494 ± 173	0.8, 0.6
Max SS firing rate (Hz)	59 ± 8.1	59 ± 8.3	51 ± 13	46 ± 7.9	52 ± 8.9	55 ± 12	57 ± 9.5	58 ± 12	1.9, 0.09
First spike latency (ms)	146 ± 86	116 ± 57	124 ± 77	91 ± 34	113 ± 79	136 ± 55	132 ± 67	142 ± 50	0.5, 0.8

Table 1. Baseline motoneuron intrinsic properties. This table summarizes all motoneurons properties analyzed in this study. Passive properties: capacitance (C_m, pF, resting membrane potential (V_m, mV, input resistance (R_{in}, MΩ), Rheobase (pA). Active properties for single action potential (AP) : threshold (AP_{TH}, mV), amplitude (AP_{AMP} ,mV), rise time (AP_{RT} ms), half width (AP_{HW}, ms) afterhyperpolarization duration ($AHP_{duration}$, ms), amplitude (AHP_{AMP}, mV) and active properties for repetitive firing : steady-state frequency-current gain (SS-F/I slope, HZ/pA), repetitive firing current threshold (TH, pA), maximum steady-state (SS, Hz) firing rate, and latency to first spike at repetitive firing current threshold, labeled in the table as first spike latency (ms). Properties of motoneurons included in each set of experiments were not different at baseline. Each column displays the number of cells and animals used in each experimental condition. Motoneuron identity was verified in a subset of experiments where cells were filled with fluorescein and verified post hoc for choline acetyltransferase (ChAT); 100% of cells were $ChAT^+$ indicating that they were indeed motoneurons. Parameters were measured with the membrane potential maintained at −75 mV by injecting bias current into motoneurons ($I_{bias\ -75}$). Experiments were only performed on cells with a stable access resistance (R_a) below 25 MΩ. Data are presented as mean ± SD and analyzed using one-way ANOVAs for each property, statistics are presented in the last column of the table.

$F_{(2,17)} = 9.6$, $p = 0.002$). Dopamine (100 µM) and the D_1 agonist increased the slope of the exponential region of the FI relationship for the first spike interval (Fig. 6G1,G2; $F_{(2,22)} = 8.4$, $p = 0.002$) and reduced the slope of the steady-state FI relationship (Fig. 6G3,G4; $H_{(2)} = 9.4$, $p = 0.009$). The reduction in steady-state slope was due to a leftward shift in steady-state FI relationship (Fig. 6G3) characterized by a reduction in the threshold for repetitive firing (Fig. 6F2; $H_{(2)} = 14$, $p < 0.001$) with no change in the maximum steady-state firing rate ($H_{(2)} = 1.4$, $p = 0.5$). These results indicate that activation of D_1 receptors elicit consistent effects as high concentrations of dopamine on motoneuron excitability and is a likely mechanism contributing to dopaminergic excitation of motor output.

Dopaminergic inhibition through D_2—receptor hyperpolarization of distributed populations of ventral interneurons. We next set out to determine the cellular mechanisms that mediate the inhibitory effects of dopamine on spinal network output with motoneurons as our first target. In contrast to our network recordings, neither low concentrations of dopamine (1–10 µM; n = 20 cells across 14 animals; Table 1) nor the D_2 agonist quinpirole (20 µM; n = 12 cells across seven animals; Table 1) altered any passive, spike or repetitive firing properties of motoneurons beyond that of the time-matched vehicle control (n = 12 cells across six animals). This remained true when we pooled motoneurons obtained from animals aged P0–2 days old (1–10 µM dopamine: n = 14; Quinpirole: n = 5) and P3–4 days old (1–10 µM dopamine: n = 6; Quinpirole: n = 7). We also considered different motoneuron types (small vs. large); however, there was no correlation between cell capacitance and changes in membrane potential elicited by low concentrations of dopamine (ΔV_m: r = −0.3, $p = 0.13$) or quinpirole ($\Delta I_{hold:}$ r = −0.1, $p = 0.72$). These results suggest that the inhibitory actions of dopamine on spinal network output are not due to D_2-receptor inhibition of intrinsic motoneuron excitability; instead, dopamine may be acting on premotor interneurons.

Property	Non-responders[a] (n = 20,8)	Responders[b] (n = 10,9)	dCINs[c] (n = 10,5)	(2,37) F, *p*
Ventral interneurons (n = 40 cells, 22 animals)				
Passive properties				
Capacitance (pF)	*47 ± 15*[b]	*73 ± 40*[a]	*46 ± 17*b	4.2, *0.02*
V_m (mV)	− 66 ± 4.3	− 66 ± 5.2	− 66 ± 6.0	0.02, 0.98
$I_{bias\ -75\ mV}$ (pA)	*− 10.8 ± 16*b	*− 57 ± 52*[a]	− 26 ± 18	4.9, *0.02*
Rin (MΩ)	759 ± 466	497 ± 248	719 ± 326	1.6, 0.1
Rheobase (pA)	84 ± 103	59 ± 13	47 ± 13	0.9, 0.4
Spike properties				
AP_{TH} (mV)	− 55 ± 4.6	− 55 ± 2.9	− 56 ± 2.3	0.2, 0.8
AP_{AMP} (mV)	71 ± 9.3	71 ± 8.2	72 ± 7.3	0.05, 0.95
$AP_{rise\ time}$ (ms)	*0.99 ± 0.48*[c]	*0.92 ± 0.3*[c]	*1.4 ± 0.25*[a,b]	4.2, *0.023*
$AP_{half\ width}$ (ms)	1.2 ± 0.5	*1.4 ± 0.6*[c]	*1.9 ± 0.4*b	6.2, *0.005*
$AHP_{duration}$ (ms)	173 ± 96	193 ± 76	172 ± 81	0.2, 0.8
AHP_{AMP} (mV)	− 4.9 ± 2.7	− 4.8 ± 2.1	− 4.8 ± 2.7	0.02, 0.98
Repetitive firing properties				
SS F/I slope (Hz/pA)	0.24 ± 0.07	0.21 ± 0.09	0.2 ± 0.1	1.0, 0.4
Repetitive firing TH (pA)	26 ± 14	31 ± 12	28 ± 13	0.5, 0.6
Max firing rate (Hz)	43 ± 16.3	39 ± 11.6	32 ± 5.9	2.1, 0.13
Fist spike latency (ms)	143 ± 81	146 ± 95	117 ± 87	0.45, 0.6

Table 2. Baseline ventral interneuron intrinsic properties. This table summarizes all interneurons properties analyzed in this study. Passive properties: capacitance (C_m, pF), resting membrane potential (V_m, mV), input resistance (R_{in}, MΩ), Rheobase (pA). Active properties for single action potential (AP): (threshold (AP_{TH}, mV), amplitude (AP_{AMP}, mV), rise time (AP_{RT}, ms), half width (AP_{HW}, ms) afterhyperpolarization duration ($AHP_{duration}$, ms), amplitude (AHP_{AMP}, mV) and active properties for repetitive firing steady-state frequency-current gain (SS-F/I slope, HZ/pA), repetitive firing current threshold (TH, pA), maximum steady-state (SS, Hz) firing rate, and latency to first spike at repetitive firing current threshold, labeled in the table as first spike latency (ms).The properties of ventral interneurons that responded to quinpirole with sustained hyperpolarization of membrane potential (V_m, responders) were compared with those that did not respond (non-responders) and also retrogradely labelled descending commissural interneurons (dCINs). Each column displays the number of cells and animals used in each experimental condition. Responders had higher capacitance and holding current than non-responders and dCINs. Parameters were measured with a membrane potential maintained at − 75 mV by injecting bias current into motoneurons ($I_{bias\ -75}$). Data are presented as mean ± SD; F and *p* values are reported from one-way ANOVAs for each property in the last column of the table. *Italic* values highlight variables where significant main effects were detected with $p < 0.05$. Superscript letters reflect significant differences between respective conditions from post hoc analysis.

Many of the premotor interneurons that produce the rhythmic activities generated by the spinal cord are distributed across lamina's VII–X of the ventral lumbar spinal cord. We next recorded from ventral interneurons located in lamina VII–X to determine a cellular locus for D_2-mediated inhibition of spinal network output (n = 30 cells across 17 animals; Table 2). Quinpirole produced a sustained hyperpolarization of the resting membrane potential in 33% of interneurons (Fig. 7B,C,D1; n = 10; dVm = − 4.8 ± 2.4 mV; two-way ANOVA, $F_{(2,37)} = 26.1$, $p < 0.0001$) and a transient hyperpolarization of membrane potential in 10% of interneurons (n = 3; dVm = − 5.16 ± 1.9 mV) that persisted for 209 ± 108 s before returning to baseline levels. The change in resting membrane potential was greater in the responders compared to non-responders (dVm responders = − 4.8 ± 2.4 mV; dVm non-responders = 1.6 ± 1.9 mV; unpaired t-test $t_{(28)} = 7.8$, $p < 0.0001$). Quinpirole reduced the input resistance (Fig. 7D2; two-way ANOVA, $F_{(2,37)} = 4.1$, $p = 0.025$) and increased the spike rise time (Fig. 7D4; two-way ANOVA, $F_{(2,35)} = 5.2$, $p = 0.01$; Dunn post hoc test, $p = 0.02$) but not the half width ($F_{(2,35)} = 2.6$, $p = 0.086$) in the group of responding interneurons ("responders"). For both responders and non-responders, quinpirole did not alter rheobase (Fig. 7D3; two-way ANOVA, $F_{(2,37)} = 0.5$, $p = 0.6$), action potential threshold (two-way ANOVA, $F_{(2,37)} = 0.3$, $p = 0.7$), AHP amplitude (two-way ANOVA, $F_{(2,37)} = 0.04$, $p = 0.96$), duration (two-way ANOVA, $F_{(2,37)} = 0.8$, $p = 0.45$), threshold for repetitive firing (two-way ANOVA, $F_{(2,37)} = 0.01$, $p = 0.98$), steady-state FI slope (Fig. 7D5: two-way ANOVA, $F_{(2,37)} = 0.9$, $p = 0.4$) or maximum steady-state firing rate (Fig. 7D6; two-way ANOVA, $F_{(3,37)} = 0.8$, $p = 0.5$). The capacitance (two-way ANOVA, $F_{(2,37)} = 4.2$, $p = 0.02$) and holding current (two-way ANOVA, $F_{(2,37)} = 4.9$, $p = 0.02$) were higher in responders than in non-responders (Table 2) and a greater proportion of responders were localized to more medial regions of spinal slices (Fig. 7B), where putative commissural interneurons reside[52]. Animal age could not account for the group of responders and non-responders. There was no difference in the age of animals from which responders (mean ± SD age: 2.7 ± 0.5 days old) and non-responders (mean ± SD age: 2.4 ± 0.8 days old; $t_{(28)} = 0.9$, $p = 0.35$) were obtained.

We next set out to determine the type of interneurons that were hyperpolarized by quinpirole. Given that many of the responding cells were located medially, we next targeted descending commissural interneurons (dCINs; n = 10 cells across five animals; Table 2) since this population can be identified based on anatomical

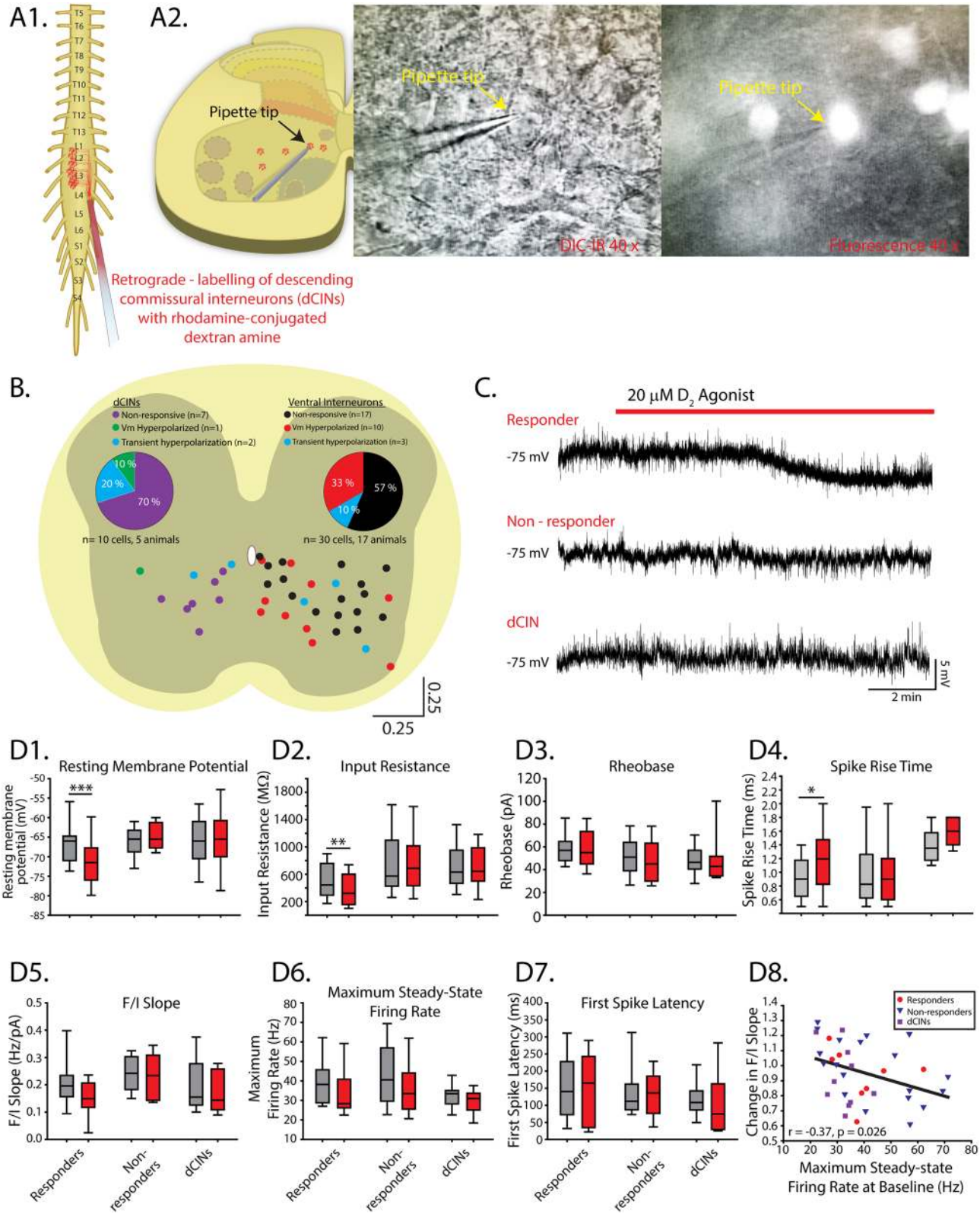
A1.
A2.
Pipette tip
Retrograde - labelling of descending commissural interneurons (dCINs) with rhodamine-conjugated dextran amine
Pipette tip
DIC-IR 40 x
Pipette tip
Fluorescence 40 x
B.
dCINs
Non-responsive (n=7)
Vm Hyperpolarized (n=1)
Transient hyperpolarization (n=2)
10 %
20 %
70 %
n= 10 cells, 5 animals
Ventral Interneurons
Non-responsive (n=17)
Vm Hyperpolarized (n=10)
Transient hyperpolarization (n=3)
33 %
57 %
10 %
n= 30 cells, 17 animals
0.25
0.25
C.
20 µM D2 Agonist
Responder
-75 mV
Non - responder
-75 mV
dCIN
-75 mV
5 mV
2 min
D1.
Resting Membrane Potential
Resting membrane potential (mV)
***
D2.
Input Resistance
Input Resistance (MΩ)
**
D3.
Rheobase
Rheobase (pA)
D4.
Spike Rise Time
Spike Rise Time (ms)
*
D5.
F/I Slope
F/I Slope (Hz/pA)
Responders
Non-responders
dCINs
D6.
Maximum Steady-State Firing Rate
Maximum Firing Rate (Hz)
Responders
Non-responders
dCINs
D7.
First Spike Latency
First Spike Latency (ms)
Responders
Non-responders
dCINs
D8.
Responders
Non-responders
dCINs
Change in F/I Slope
r = -0.37, p = 0.026
Maximum Steady-state Firing Rate at Baseline (Hz)

◀ **Figure 7.** D_2 agonists hyperpolarize a proportion of ventral interneurons. Whole-cell recordings obtained from lamina VII–X interneurons. (**A1**) Descending commissural interneurons (dCINs) were retrogradely labelled with rhodamine-conjugated dextran amine crystals inserted into the ventrolateral funiculus at L4 level. (**A2**) Cells were visualized in transverse lumbar slices under infrared differential interference contrast (IR-DIC) or epifluorescent illumination. (**B**) Ventral interneuron location was measured relative to the central canal and X–Y positions normalized to the distance of ventral and lateral borders of lumbar slices. (**C**) Whole-cell current-clamp recordings depict responsiveness of interneuron resting membrane potential to the D_2 agonist (quinpirole, 20 μM) in responders, non-responders, and dCINs. A proportion of ventral interneurons responded to quinpirole with either a sustained (**B**, red and green dots) or transient (**B**, blue dots) hyperpolarization of the membrane potential. A reduction in input resistance and increase in spike rise time accompanied hyperpolarization in sustained responders (**D2**, **D4**). Box and whisker plots display interquartile range (boxes), median (horizontal black lines), max, and minimum value in data range (whiskers). asterisks denote significance level from post hoc tests (*$p < 0.05$, **$p < 0.01$, ***$p < 0.001$) following two-way ANOVA. (**D8**) Reductions in steady-state frequency-current (**FI**) slope of all cells following application of quinpirole was greatest in cells that had a higher maximum steady-state firing rate at baseline.

connectivity[53,54], display intrinsic burst properties[55] and are rhythmically-active during neurochemically-evoked fictive locomotion[56]. dCINs were retrogradely labelled with tetramethylrhodamine-conjugated dextran amine (molecular weight (MW) 3000; Molecular Probes, Inc.) inserted into the ventrolateral funiculus at the L4 segment (Fig. 7A). In contrast to our hypothesis, only one dCIN responded with a sustained hyperpolarization and two were transiently hyperpolarized (Fig. 7B) by quinpirole. Quinpirole did not alter any passive, spike, or repetitive firing properties of dCINs (n = 10; Fig. 7D). These data suggest that the dCINs, although responsive in similar proportions to our global interneuron survey, do not exclusively account for the 33% responding group and, therefore, are likely, not responsible for the observed network effects. Interestingly, when all interneuron data were pooled (n = 40 cells), irrespective of responsiveness as indicated by changes in resting membrane potential, quinpirole had the greatest effect in cells that had a higher maximum steady-state firing rate at baseline (Fig. 7D8; $r = -0.37$, $p = 0.026$). There was no correlation between baseline FI slope and changes in FI slope in response to quinpirole ($r = -0.09$, $p = 0.6$).

While dCINs can be identified anatomically, they are heterogeneous with respect to their neurotransmitter phenotype[57] and as a result have varying contributions to network activities[52,56,58]. We therefore next targeted V3 interneurons which are exclusively glutamatergic, contribute to the stabilization of locomotor-like rhythmicity and can be identified genetically based on the expression of the Sim1 transcription factor[59]. Heterogeneity with respect to location, morphology and electrophysiological properties has also been reported in V3 interneurons[60,61] which may be accounted for in part by a recently described hierarchical microcircuit whereby a medial population projects to a lateral population which provide glutamatergic excitation of ipsilateral motoneurons. Both populations also project commissurally and receive recurrent glutamatergic inputs from intra and intersegmental ipsilateral motoneurons[62]. Given that dopamine inhibits ventral root-evoked locomotor activity, which may be mediated by this circuit[63], through D_2-receptor signaling[29], we hypothesized that V3 interneurons may be a cellular locus for D_2-mediated inhibition of spinal network activity.

Consistent with our global interneuron survey, quinpirole produced a sustained hyperpolarization of the resting membrane potential in a proportion of V3 interneurons (n = 5 cells; 27%) that we recorded from (total V3 interneurons n = 23 cells, 7 animals) and transient hyperpolarization in 3 (13%) V3 interneurons. The magnitude of the response in the 5 cells that responded with a sustained hyperpolarization was variable and approached, but did not reach significance (Supp. Figure 1; paired t-test: $t_{(4)} = 2.5$, $p = 0.06$); however, did reach significance when the cells that responded with a transient hyperpolarization were included in the analysis (paired t-test: $t_{(6)} = 2.7$, $p = 0.03$). Consistent with our global interneuron survey the change in resting membrane potential elicited by quinpirole was significantly greater in responding (n = 5; dVm = -1.9 ± 1.9 mV) compared to non-responding (n = 15; dVm = -0.3 ± 1.0 mV) V3 interneurons (unpaired t-test: $t_{(16)} = 3.8$, $p = 0.002$).

Discussion

Dopamine is a monoamine neuromodulator that is important for the control of rhythmically active motor circuits across phyla (reviewed by Ref.[8]) but is probably best known in vertebrates for the control of dedicated circuits in the basal ganglia that control action selection (reviewed by Ref.[64]). Work in small circuits of invertebrates has established that circuit connectomes define the constraints on which networks operate and that neuromodulators diversify outputs by altering intrinsic and synaptic properties of the neurons that compose the circuit (for reviews see Refs.[1–3]). In line with this, the distribution of receptors within circuits constrain the effect of neuromodulators on circuit output. For example, dopamine is exclusively inhibitory in spinal circuits of *Xenopus* tadpoles prior to free-swimming stages[65] due to expression of D_2 but not D_1 receptors. We show that dopamine has bidirectional concentration-dependent effects on spinal network output in neonatal mice where all dopamine receptor types are expressed[20,31,32] which is consistent with what has been reported in tadpoles at free swimming-stages[12]. Our data highlights that neuromodulator concentration is also important because receptors have varying ligand affinities which underlie concentration-dependent actions of modulators which is consistent with other work demonstrating opposite effects on spinal network output through activation of opposing receptor subtypes (Reviewed by Ref.[34]). This includes opposing actions of serotonergic 5-HT_7/$5HT_{2a}$ and $5HT_1$ receptors[66] , noradrenergic α-1 and α-2 receptors[66,67] and cholinergic M_2 and M_3 receptors[43,68]. Although dopamine predominantly inhibits spinal output in neonatal mice, similar to pre-free swimming tadpoles and larval zebrafish[69], it is primarily due to the concentration of spinal dopamine, not the distribution of receptors. Our previous work has shown that

neuromodulation of mammalian spinal networks is dependent on network excitability state[13] which is consistent with findings from invertebrates[14,15]. Our current work builds upon ours and extends that of others that demonstrate bi-directional control of spinal networks by noradrenaline[66,67], serotonin[66] and acetylcholine[43,68] and shows that receptor mechanisms and concentration-dependent control of spinal network output is also state-dependent. This is important because receptor expression, modulator concentration and network excitability are not fixed and fluctuate dynamically[70,71]. Therefore, these three factors need to be considered if we wish to understand how networks create diverse neuromodulator-dependent outputs (Fig. 8A).

A physiologically silent excitatory D_1 pathway? Previous work has shown predominantly excitatory D_1-receptor mediated effects of dopamine on fictive locomotion which is characteristic of the network operating in a high excitability state[13]—albeit in these studies, higher concentrations of dopamine are necessary to elicit observable effects[20–23,30,31]. Here, we show that endogenous levels of dopamine within the spinal cord of neonatal mice are low. Even though HPLC suggests low concentrations of dopamine in the neonatal spinal cord, a critical question that we addressed is what would happen when we manipulated endogenous dopamine? We accomplished this by blocking dopamine reuptake and metabolism and found that the effects were not excitatory, but inhibitory. Based on this, we suggest that although present, the excitatory D_1-mediated pathway is 'physiologically silent' during early postnatal stages given that endogenous levels are not sufficient to activate this pathway. A similar phenomenon has been reported for glutamatergic synapses in developing circuits of the hippocampus which express NMDA but not AMPA receptors. As a result, glutamatergic synapses fall 'physiologically silent' as the release of glutamate does not produce sufficient depolarization of the postsynaptic membrane to remove the magnesium block from the pore of the NMDA channel[72,73].

Excitability state also influences the receptor mechanisms and therefore concentration-dependent control of modulators on network output. In the spinal cord, D_1 pathways may be more important for the regulation of spinal circuits operating in higher excitability states. For example, fictive locomotor rhythms are drastically impacted when D_1 receptors are manipulated whereas manipulation of D_2 receptors elicit only subtle changes in rhythm frequency, with rhythm robustness being maintained[31] (Fig. 8B2). In the adult animal; however, network excitability increases, and spinal dopamine levels are higher due to increases in descending inputs (Fig. 8B1). In line with this, optogenetic activation of the dopaminergic A11 leads to an increase in motor activity[74]. Similarly, the excitatory D_1 system is more important for the control of stepping movements whereas the inhibitory D_2 system plays less of a role[21,75]. Instead, the inhibitory D_2 pathway may be more important in maintaining network quiescence during periods of immobility such as has been inferred by the study of firing patterns in the zebrafish[9] (Fig. 8B1). Our data demonstrates that in the neonatal mouse, where spinal dopamine levels and network excitability are low, that inhibition of motor output prevails (Fig. 8B2). Thus, this points to the receptor-specific and therefore concentration-dependent control of modulators on network output being strongly influenced by the state of the network on which they are acting.

Dedicated network components segregate excitatory and inhibitory control of spinal networks. Dedicated circuits regulated by non-overlapping populations of neurons that express D_1 and D_2 receptors compose the direct and indirect pathways of the basal ganglia in vertebrates and have also been reported in the superior colliculus of rodents[76]. Our work suggests dedicated network elements within the spinal cord that are regulated by D_1 and D_2 pathways (Fig. 8B3). Specifically, we found that D_1 receptors excite motoneurons through similar mechanisms that have been previously reported[50,51], but are not affected by low concentrations of dopamine or D_2 agonists. This points to the possibility of a dedicated D_1-dependent circuit that could underlie the generation of rhythmic activities elicited by high concentrations of dopamine. Motoneurons compose key rhythm generating elements in invertebrate circuits[77–79] and also participate in rhythm generation in vertebrates[80], including rodents[42,62,63,81,82]. V3 interneurons are one subclass of genetically-defined spinal interneuron that are important for the generation of rhythmic activities in mammalian spinal networks[59,61,83] and receive recurrent excitatory collaterals from motoneurons in rodents[62]. Motoneurons in the rodent spinal cord also form glutamatergic synaptic connections amongst each other[82] and activation of D_1 receptors could serve to synchronize motor pools. Previous results demonstrating D_1- and not D_2-mediated increases in AMPA conductances on motoneurons[51] support this possibility. We cannot rule out the possibility that there is a degree of overlap between D_1 and D_2 controlled network elements within the spinal cord. While we did not examine the D_1 control of ventral interneurons, we did find that D_2 receptors hyperpolarize a subset of V3 interneurons. This population is therefore a potential cellular locus where cooperative excitatory D_1–D_2 interactions that we report here could occur. D_1 and D_2 receptors have been reported in the brain to become co-activated or form heterodimeric complexes that augment neuronal excitability through PLC-dependent increases in intracellular calcium[37–40]. Whether D_1 and D_2 receptors form protein–protein interactions or heterodimers is controversial and our immunoprecipitation results should be interpreted with caution. D_1 receptors have been demonstrated to form heteromeric interactions with A_1 adenosine receptors[84] which may underlie the D_1-dependence over which glia control motoneuron excitability and locomotor network activity through the release of adenosine[23,85]. Our pharmacological data indicates that co-activation of D_1 and D_2 receptors may enhance the excitatory effects of dopamine in the neonatal mouse spinal cord which is consistent with reports in the cultured neonatal striatal neurons[38,40] and pyramidal neurons of the juvenile but not adult lateral orbitofrontal cortex[39]. This notion is supported by our experiments that show blockade of the excitatory effect of dopamine by D_2 antagonists and enhancement of the excitatory effect of a D_1 agonist when co-applied with a D_2 agonist. As higher concentrations of dopamine are required to elicit an excitatory effect, this pathway may be physiologically silent during early postnatal development; however, increasing dopamine concentrations at later stages may activate this pathway.

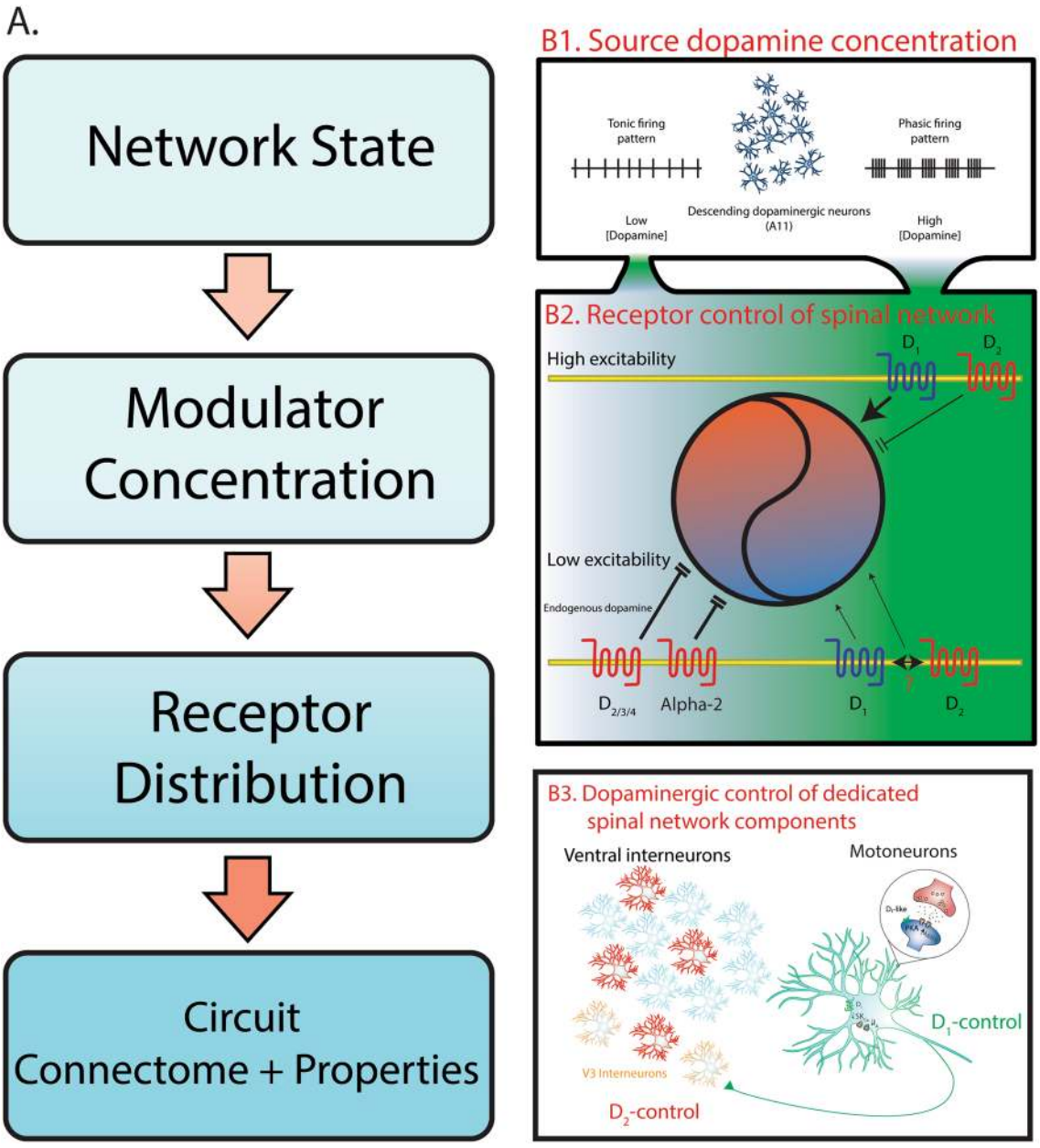

Figure 8. Dopamine exerts state and receptor-dependent control of spinal motor networks. (**A**) Neural network output is dependent on multiple factors. Circuit connectomes and intrinsic properties defining constraints of a network output. Similarly, the distribution of neuromodulator receptors define the constraints on which neuromodulators can alter these properties. Varying ligand affinities of these receptors determine the dose-dependent effect of neuromodulators and network state dictates the dose-dependent effects of neuromodulators. (**B1**) Previous work has demonstrated that tonic and phasic firing patterns of dopamine cells lead to the release of low and high concentrations of dopamine, respectively[10]. (**B2**) During a low excitability state (blue part of the circle), low concentrations of dopamine (denoted by the green gradient) acted on D_2, D_3, D_4 and α_2-adrenergic receptors in parallel to inhibit (parallel stop lines) spinal motor output. As dopamine levels rise, activation of D_1 and co-activation of D_2 receptors increase (arrowheads) spinal network output. During a high excitability state (orange part of the circle), the actions of low dopamine are not apparent and at higher concentrations, activation of D_1 receptors boost spinal network output and activation of D_2 receptors slows rhythmic activity [13]. (**B3**) Higher concentrations of dopamine act through D_1 receptors to increase motoneuron excitability by reducing A-type and SK_{Ca}-dependent calcium currents [50]. D_2-mediated inhibition of spinal network output is triggered by reduced excitability in a proportion of ventral interneurons (red cells).

The inhibitory D_2 pathway on the other hand does not appear to act through the modulation of motoneuron intrinsic or synaptic properties[51] but instead hyperpolarizes a proportion of ventral interneurons. Based on our responsiveness criteria, a majority of cells that responded to a D_2 agonist with sustained hyperpolarization of the membrane potential were localized more medially in lumbar slices. We tested the hypothesis that a subpopulation of interneurons was D_2 sensitive and tested both dCINs and genetically identified V3 interneurons. Our hypothesis was not supported, and similar proportions of D_2 sensitive interneurons were found, even within a subpopulation of genetically defined interneurons. Our data suggest that there is heterogeneity in the responsiveness to neuromodulators within a class of genetically defined interneurons and that D_2 actions may not be localized to a particular class of interneurons. One possibility is that neuromodulators elicit a robust effect on network output through distributed control across multiple classes of genetically-defined interneurons which would be consistent with findings that the locomotor rhythm generator is also distributed across several classes of interneurons[86–88]. Our network data suggests that low concentrations of dopamine inhibit network output by acting in parallel on D_2, D_3, D_4 and α_2 receptors. This dependence on the $D_{2–4}$ receptors for inhibition matches the fact that none of the inhibitory receptors show uniform expression in the ventral horn (Allen Mouse Spinal Cord Atlas). One caveat is that we may have underestimated the cellular targets that underlie dopamine's robust inhibitory effect on the network given that in this series of experiments we looked at the activation of D_2 receptors alone. Alternatively, D_2 receptors may modulate synaptic transmission in presynaptic contacts from premotor to motoneuron synapses similar to observations in the striatum[89]. Our previous work suggests a presynaptic role for D_2 receptors in depressing recurrent collateral mediated excitation[29], and others have also established a dopamine-mediated depression of the monosynaptic reflex[90]. Given our current data showing little effects of D_2 receptors agonists on intrinsic properties together with previous work, this supports a D_2 receptors mediated presynaptic role.

Developmental considerations for the endogenous dopaminergic system. Our analysis of dopaminergic regulation of spontaneous network activity and spinal neuron excitability spanned an age range from postnatal days 0 to 4. Spontaneous network activity generated during embryonic development is critical for maturation of spinal networks[18] and has been reported to decrease over the first postnatal week as spinal networks mature[16]. The reduction in spontaneous network activity is paralleled by differential maturation of flexor and extensor motoneurons during the first 6 postnatal days in the rat[91] and reduced passive excitability and diversification of mouse motoneuron intrinsic properties[44,46,92,93] leading into the second postnatal week as weight-bearing locomotion begins to emerge. Consistent with this, we find an increase in whole cell capacitance of motoneurons when comparing cells obtained from animals age P0-2 days old to animals age P3–4 days old. Intrinsic properties of different classes of genetically-defined interneurons also undergo intrinsic property diversification during this time (Shox2:[94]; V2a:[95]; V3:[61]). A robust inhibitory endogenous dopaminergic system may act as a brake on premotor network activity during perinatal development when passive excitability of motoneurons is relatively high[44,46,92,93] and chloride-mediated synaptic transmission still causes partial depolarization[96]. An inhibitory brake would prevent runaway excitation of spinal network activity during this critical period of development. A robust background inhibitory system mediated by the parallel inhibitory action of D_2, D_3, D_4, and α_2-adrenergic receptors activated by low levels of endogenous dopamine would counteract depolarizing chloride-mediated transmission[96].

The dopamine receptor expression profile amongst different populations of spinal neurons is also likely to change during postnatal development, and indeed this is the case in *Xenopus* tadpoles[12,65] and the larval zebrafish[69,97]. Signaling through D_2-like receptors may also play a role in driving the maturation of spinal networks. In larval zebrafish, D_4 receptors drive the maturation of spinal locomotor network organization[98] and function leading to changes in locomotor behaviour[99]. Similar processes may also occur perinatally in rodents, in that the preferential activation of the D_2 receptor system may favour intracellular signaling that results in network reorganization. Serotonin receptors have been found to shape network function and inhibitory synaptic transmission during early postnatal days of rodents[100,101]. Dopamine could, therefore, act analogously via the D_2-system during perinatal development. Our results provide insight into the functional expression of dopamine receptors in spinal neurons during this critical stage in postnatal development. Our results indicated that D_2 receptors are distributed across ventral interneurons and D_1 but not D_2 receptors are functionally expressed in motoneurons at this stage in development. However, we did not explore D_1 regulation of ventral interneuron excitability, and indeed high concentrations of dopamine have been reported to augment rhythmicity in glutamatergic Hb9 interneurons[50]. Future work exploring expression and function of D_1 receptors in ventral interneurons may provide insight into populations that underlie the diverse rhythms and modulation of network output by dopamine in vitro[13,20,22,23,25,31]. These works will serve as a foundation to explore modulation of spinal circuits during later stages of postnatal development into adulthood, approaching freely behaving stages around the third postnatal week and when descending dopamine systems are fully mature by P21[102].

Caveats. A caveat of our results is that many of our experimental approaches rely on pharmacological manipulations of target receptors. Indeed dopamine itself has been demonstrated in other regions of the brain to be cross-reactive with non-dopamine receptors and in some instances, to be converted to serotonin or noradrenaline by presynaptic neurons and can alter the activity of other monoamine-releasing neurons[103]. Consistent with this notion, we demonstrate that the inhibitory action of low dopamine is mediated in part by α_2 noradrenergic receptors, therefore conversion to noradrenaline or activation of endogenous sources of noradrenaline cannot be excluded. While we did not test the contribution of non-dopamine receptors to the excitatory effect of high dopamine, it remains a possibility. In addition many of the agonists/antagonists we employed have known affinities for non-dopamine receptors. For example, the D_1-agonist we employed has known affinities as a partial

agonist for the $5HT_{2c}$ receptor[104–106] and antagonist for the $5HT_{2a}$ receptor[107]. That said, collectively, our results are consistent with our hypotheses—agonists reproduce the effects of low and high dopamine and their effects can be blocked by respective antagonists. In all likelihood, neuromodulatory systems of the spinal cord do not operate in isolation, but in parallel to globally regulate spinal network function. There is evidence for this in the stomatogastric nervous system of the crab/lobster therefore, cooperation amongst neuromodulatory systems may be more important than their individual actions. In light of our previous work[13], cooperation amongst neuromodulatory systems may provide degeneracy with respect to the mechanisms for moving the network through various excitability states.

Conclusions. Here we present evidence for an inhibitory physiological role of dopamine in the regulation of developing mammalian spinal networks. We also demonstrate an excitatory D_1-mediated pathway that acts through excitation of motoneurons, and possibly recurrent excitatory collaterals to CPG neurons, however given that endogenous levels of dopamine are low, we propose that this pathway is physiologically silent at the developmental stage studied here (P0–4). These data advance our understanding of how neuromodulators regulate network output in light of dynamically changing modulator concentrations and levels of network excitability.

Methods

Tissue preparation. We anesthetized all animals by hypothermia. Pups were decapitated and eviscerated to expose the vertebral column and rib cage. The isolated vertebrae and rib cage were transferred to a dish lined with a silicone elastomer (Sylgard; DowDuPont, Midland, MI) and perfused with room-temperature (21–23 °C) carbogenated (95% O_2/5% CO_2) aCSF (in mM, 4 KCl, 128 NaCl, 1 $MgSO_4$, 1.5 $CaCl_2$, 0.5 Na_2HPO_4, 21 $NaHCO_3$, 30 D-glucose; 310–315 mOsm.). We exposed the spinal cord with a ventral laminectomy and isolated it by cutting the nerve roots that connected it to the vertebral column. The isolated spinal cord was then transferred to a recording chamber, perfused with carbogenated aCSF, and placed ventral side up. The bath temperature was gradually increased to 27 °C, to be closer to the physiological temperature in vivo, and to ensure that the preparation temperature was locked at a level above fluctuating room temperature[30]. We let the spinal cords stabilize for 1 h before performing experiments.

Spinal cord slice preparation. Following isolation, spinal cords were transected above the tenth thoracic (T10) and below the first sacral (S1) segments and transferred to a slicing chamber. Pre-warmed liquefied 20% gelatin was used to secure cords to an agar (3%) block that was glued with cyanoacrylate to the base of a cutting chamber and immersed in ice-cold, carbogenated, high-sucrose slicing aCSF (in mM, 25 NaCl, 188 sucrose, 1.9 KCl, 10 Mg SO_4, 1.2 Na_2HPO_4, 26 $NaHCO_3$; 25 D-Glucose; 340 mOsm). Using a vibratome (Leica, Bussloch, Germany) we cut 250-µm-thick lumbar slices, collected and transferred them to a recovery chamber containing regular carbogenated aCSF (see Tissue Preparation) heated to 32 °C for one hour, then maintained them at room temperature for at least 30 min before transferring them to a recording chamber.

Labelling of descending commissural interneurons (dCINs). We retrogradely labelled dCINs by inserting tetramethylrhodamine-conjugated dextran amine crystals (MW 3000; Molecular Probes, Inc.) into a cut in the ventrolateral funiculus at the L4 segment. Spinal cords recovered for 4 h to allow retrograde uptake of the fluorescent dye. Fluorescently labelled cells were visualized with epifluorescent illumination.

Electrophysiological recordings. Extracellular neurograms were recorded by drawing ventral roots of the second (L2) and fifth (L5) lumbar segments into tight-fitting suction electrodes fashioned from polyethylene tubing (PE50). Signals were amplified 1000× in total via 10× pre-amplification and 100× second-stage amplification (Cornerstone EX4-400 Quad Differential Amplifier; Dagan Corporation, Minneapolis, MN). Amplified signals were band-pass filtered (0.1–1000 Hz) and digitized at 2.5 kHz (Digidata 1440A/1550B; Molecular Devices, Sunnyvale, CA). Data were acquired in Clampex 10.4/10.7 software (Molecular Devices) and saved on a Dell computer for offline analysis. All experiments were performed on spinal cords naïve to drugs and experimental treatment.

Whole-cell patch-clamp recordings. Spinal cord slices were gently transferred to a recording chamber perfused with room-temperature carbogenated recording aCSF (in mM, 128 NaCl, 4 KCl, 1.5 $CaCl_2$, 1.0 $MgSO_4$, 0.5 Na_2HPO_4, 21 $NaHCO_3$, 30 D-glucose; approximately 310 mOsm) and stabilized in the recording dish with a stainless-steel harp. We gradually heated aCSF to 27 °C. Slices were visualized (Olympus BX51WI; Olympus Corporation, Tokyo, Japan) under 5× magnification and putative motoneurons identified using a 40× objective with infrared differential interference contrast (IR-DIC) illumination. We identified putative motoneurons based on their location in the ventrolateral spinal cord and a soma diameter of greater than 20 µm. A cohort of motoneurons was passively filled with fluorescein dextran amine (FITC; MW 3000; 200 µM; Molecular Probes, Inc.) added to the intracellular solution to visualize and localize the recorded cells, for 20–60 min and motoneuron identity was verified post hoc by performing immunohistochemistry for choline acetyltransferase (ChAT)[45]. To verify motoneuron identity in subsequent experiments, basal biophysical properties of putative motoneurons were compared with a cohort (n = 8) of FITC-filled ChAT-positive cells and are included in Supp. Fig. 2. We identified no differences in basal biophysical properties of ChAT-positive identified cells, compared with cells in other experiments identified by position and size (Table 1). In one set of experiments, we recorded from ventral interneurons in lamina VII–X, descending commissural interneurons (dCINs) and V3 interneurons of the lumbar spinal cord (Table 2). We measured the distance of each interneuron from the central canal (LinLab2;

Scientifica, Uckfield, UK) and normalized position, relative to lateral and ventral borders, and plotted the normalized positions on a template transverse spinal cord. Responsiveness was determined by the change in resting membrane potential. All experiments were performed on one cell per slice to ensure that all cells were naïve to treatment.

Recording electrodes were pulled from borosilicate capillary tubes (O.D. = 1.5 mm, I.D. = 0.86 mm) using a Flaming/Brown Model P-97 micropipette puller (Sutter Instrument, Novato, CA). Pipettes pulled to record from motoneurons, and interneurons were within the range of 3–5 MΩ and 6–9 MΩ, respectively. Pipettes were backfilled with intracellular solution (in mM, 130 K-gluconate, 0.1 EGTA, 10 HEPES, 7 NaCl, 0.3 $MgCl_2$, 2 ATP, 0.5 GTP, 5 phosphocreatine; 280 mOsm). Intracellular solutions were balanced to a pH of 7.3 with 10 M KOH and osmolality was cross-checked to fall within the range of 275–290 mOsm. Data were acquired at 10 kHz using Clampex software (PClamp 10.4; Molecular Devices).

We examined intrinsic properties of motoneurons and ventral interneurons and terminated experiments if access resistance was greater than 25 MΩ for motoneurons and 35 MΩ for interneurons, if cells had a resting membrane potential greater than − 50 mV, or if action potential amplitude was less than 60 mV at baseline. Cells were excluded from analysis if access resistance deviated by more than 20% by the end of the recording. Membrane potential was maintained at approximately − 75 mV during experiments, after correcting for a liquid junction potential of 14.3 mV. The liquid junction potential was calculated in Clampfit (PClamp 10.4; Molecular Devices), using the ionic composition of our extracellular and intracellular solutions. Protocols for the examination of intrinsic properties have been described elsewhere [92].

Pharmacology. Dopamine hydrochloride (Sigma-Aldrich, Inc., St. Louis, MO) was bath applied in separate experiments at 1 μM, 3 μM, 10 μM, 30 μM, 100 μM, and 300 μM to determine dose-dependent effects on motor activity. The receptor-selective agonists we used included SKF 81297 for D_1-like receptors (10–50 μM; Tocris, Minneapolis, MN); quinpirole for D_2-like receptors (10–50 μM; Tocris); and the D_1/D_2 receptor co-agonist SKF 83959 (10–50 μM; Tocris). For dopamine receptor antagonists we used the D_1-like antagonist SCH-23390 (10 μM; Tocris); the D_2-like antagonists sulpiride (20 μM) and L-741626 (12 μM); the selective D_3 receptor antagonist SB 27701A (5 μM; Tocris); the selective D_4 receptor antagonist L-745870 (5 μM; Tocris). We also used the α_2 adrenergic receptor antagonist, yohimbine (2–4 μM; Tocris). Endogenous dopamine levels were manipulated with the DAT inhibitor GBR-12909 (10 μM; Hello Bio, Princeton, NJ) and the monoamine oxidase A and B inhibitor bifemelane (50 μM; Tocris).

Immunoprecipitation for D_1 and D_2 receptors. Spinal cords were dissected from neonatal mice (age P0–4) in ice-cold (4–8 °C) aCSF and homogenized in lysis buffer containing 50 mM TrisHCl, 150 mM NaCl, 10 mM EDTA, 0.1% Triton-X, and 5% Glycerol. Lysis buffer contained protease inhibitors (Sigma) and phosphatase inhibitors (GBiosciences). We homogenized three spinal cords in 100 μL of buffer and incubated them on ice for 1 h before centrifuging them at 10,000 rpm for 30 min at 4 °C. Lysates were then extracted and stored at − 20 °C.

To reduce nonspecific binding, we first incubated lysates in anti-rabbit Ig agarose beads (Trueblot; Rockland Inc., Limerick, PA) for 30 min, on ice and in the absence of primary antibody. We then removed the supernatant and incubated the lysates on ice for 1 h with rabbit antibody to D_2 receptors (1 μg per 100 μL, Millipore). Anti-rabbit Ig IP beads were added, and samples were incubated overnight at 4 °C with gentle agitation. Immunoprecipitates were washed with lysis buffer, heated in loading buffer (350 mM Tris, 30% glycerol, 1.6% SDS, 1.2% bromophenol blue, 6% β-mercaptoethanol) to 95 °C for 10 min, electrophoresed on a precast SDS gel (4–12% Tris HCl; BioRad, Hercules, CA), and transferred onto a nitrocellulose membrane. After blocking, the membranes were incubated with guinea pig antibody to D_1 receptors (1:400; Alomone, Jerusalem, Israel) and rabbit antibody to D_2 receptors (1:500; Millipore, Burlington, MA), washed, incubated for 2 h at room temperature in fluorophore-conjugated secondary antibodies (IRDye anti-guinea pig and Trueblot anti-rabbit IgG DyLight, 1:1000), and visualized via antibody fluorescence at 680 or 800 nm (Odyssey CLx; LI-COR Biosciences, Lincoln, NE). Full length unprocessed images can be found in Supp.Fig. 3.

Post hoc verification of motoneurons. Following the completion of experimental protocols, we post-fixed slices overnight in 4% paraformaldehyde (PFA) at 4 °C, washed them the next morning in phosphate-buffered saline (PBS) for three 20-min intervals, and stored them at 4 °C. On the day we performed immunohistochemistry, we first washed the slices for 30 min (3 × 10 min) in PBS with 0.5% Triton-X 100 (PBST) then incubated them at room temperature (21–23 °C) for 6 h in blocking solution containing 10% donkey serum in 0.5% PBST. Primary antibodies for choline acetyltransferase (ChAT) (1:500; goat anti-ChAT; Millipore Cat No. AB144) and the fluorescence marker (1:1000; rabbit anti-FITC, ThermoFisher Cat No. 11090) were diluted in blocking solution and the slices incubated with them for at least 24 h at room temperature. Slices were then washed in PBST (0.5%) for 80 min (4 × 20 min) at room temperature before secondary antibodies (donkey anti-rabbit Alexa Fluor 1:1000, Life Technologies Cat No. A-21206; Donkey anti-Goat Alexa 568 1:1000; Cat No. A21447, Life Technologies, Carlsbad, CA) were applied for 4–8 h at room temperature, then washed for 80 min in PBST (0.5%). Slices were mounted and cover slipped with fluorescent mounting medium (Vectashield; Vector Laboratories, Burlingame, CA); coverslips were separated from slides by 500 μm spacers to prevent crushing.

Imaging. All sections processed via immunohistochemistry were imaged on a Nikon A1R MP^+ microscope (Nikon, Tokyo, Japan) operating in confocal mode with a 16 × water-immersion objective lens (numerical aperture [NA] = 0.8, working distance [WD] = 3 mm). Image acquisition used a z-step of 1 μm and averaged two frames with a resolution of 2048 × 2048. Pixel dwell time was 2.5 ms and exposure settings were maintained for

all sections. We used NIS-Elements software (Nikon) for image acquisition and ImageJ to perform maximum intensity projections of z-stacks.

High-performance liquid chromatography. Monoamine content of neonatal and adult spinal cords was measured using high-performance liquid chromatography (HPLC). We dissected spinal cords from neonatal (P3, n = 11) C57BL/6 mice in aCSF as described above and extracted adult spinal cords (P60, n = 17) with a pressure ejection method. Tissue was then flash-frozen with liquid nitrogen, stored at − 80 °C, and analyzed for biogenic amines with a modified version of our previously-published HPLC method[108]. Tissue was homogenized in ice-cold 0.1 M perchloric acid containing EDTA (10 mg%) and ascorbic acid (50 µM). We centrifuged the homogenate and used 10 µl of supernatant in the assay. The HPLC system consisted of a Waters Alliance 2695 XE Separations Module equipped with a Waters Atlantis dC18 3 µm (3.0 × 100 mm) analytical column and a Waters 2465 electrochemical detector with an applied potential set at 0.64 V. The mobile phase was composed of 55 mM monosodium phosphate, 850 µM sodium octyl sulfate, 470 µM EDTA, 8% acetonitrile and 2 mM sodium chloride in water, with the pH adjusted to 2.9. The mobile phase flow rate was 0.6 ml/min. Retention times (in min) were 8.6 (NE), 16.2 (DA) and 39.2 (5-HT).

Data analysis. We determined the relative inhibitory or excitatory effects of dopamine and dopamine receptor agonists on spontaneous motor network activity using methods similar to those in our previous work[31]: we calculated a response ratio from single ventral root neurograms between the root mean square of 5 min of basal spontaneous activity and 5 min of activity recorded 20 min after adding the drug. We subtracted 1 from the response ratio so that positive values reflect excitation and negative values reflect inhibition. The response ratio was used as a high throughput assay to detect global changes in network activity. Neurogram data were analyzed with Spike2 software. Bursts of spontaneous activity were analyzed using Clampfit (Molecular Devices) to determine how episode number and amplitude contributed to changes in response ratio. Spectral analyses were conducted using Spinalcore software[109] whenever we detected excitatory changes or observed rhythmicity.

Patterns of rhythmic motor activity recorded from single ventral roots were analyzed with autowavelet spectral analysis. We created and analyzed frequency–power spectrograms by selecting regions of interest around frequency ranges that coincided with those in the raw neurogram. The spectrograms revealed two high power regions that reflect distinct rhythms evoked by dopamine at high concentrations: a slow 0.01–0.04 Hz rhythm and a fast 0.8–1.2 Hz rhythm. Regions of interest were selected within these frequency ranges and analyzed over the time course of each experiment. Frequency power within selected regions of interest that corresponded to the fast and slow rhythms were used as a measure of rhythm robustness. Data were segmented into 30 s bins and averaged over 5-min intervals for statistical analysis. We used tools available in Spinalcore for all analyses of rhythmic motor activity[109], consistent with Sharples and Whelan[13].

Motoneuron and interneuron intrinsic properties measured during whole-cell patch-clamp experiments were analyzed as in our previous work[45,50,92], with the exception of repetitive firing analyses, which examined the instantaneous firing rate for the first spike interval and steady-state firing separately.

Experimental design and statistical analysis. All experiments were repeated measures. We tested for differences in the magnitude of effects between conditions with one-way ANOVAs, focusing on comparisons to time-matched vehicle controls. Two-way ANOVAs compared baseline to multiple post-drug conditions. All effects surpassing a significance threshold of $p < 0.05$ were further examined with post hoc analyses. We used Holm-Sidak post hoc tests to compare all treatment conditions to the appropriate normalized time-matched vehicle control. Data that violated assumptions of normality (Shapiro–Wilk test) or equal variance (Brown–Forsythe test) were analyzed via nonparametric Mann–Whitney *U* (if two groups) or Kruskal–Wallis (if more than two groups) tests.

Ethical approval and animals. Experiments were performed on male and female neonatal (P0–P4, n = 262) C57BL/6 mice. High performance liquid chromatography (HPLC) was also performed on a cohort of adult (P60, n = 17) C57BL/6 mice. A subset of experiments were performed on spinal cord slices obtained from neonatal (P0–4, n = 7) *Sim1*$^{Cre/+}$; *Rosa*^{floxstop26TdTom} which were used to visualize and record from V3 interneurons. All methods were carried out in accordance with relevant guidelines and regulations by the University of Calgary Health Sciences Animal Care Committee and the University Committee on Laboratory Animals at Dalhousie University. Also, all procedures performed were approved by the University of Calgary Health Sciences Animal Care Committee and the University Committee on Laboratory Animals at Dalhousie University.

Received: 24 February 2020; Accepted: 11 September 2020
Published online: 02 October 2020

References

1. Miles, G. B. & Sillar, K. T. Neuromodulation of vertebrate locomotor control networks. *Physiology* **26**, 393–411 (2011).
2. Marder, E. & Thirumalai, V. Cellular, synaptic and network effects of neuromodulation. *Neural Netw.* **15**, 479–493 (2002).
3. Stein, W. Modulation of stomatogastric rhythms. *J. Comp. Physiol. A Neuroethol. Sens. Neural Behav. Physiol.* **195**, 989–1009 (2009).
4. Grillner, S. & Robertson, B. The basal ganglia over 500 million years. *Curr. Biol.* **26**, R1088–R1100 (2016).

5. Kravitz, A. V. *et al.* Regulation of parkinsonian motor behaviours by optogenetic control of basal ganglia circuitry. *Nature* **466**, 622–626 (2010).
6. Bateup, H. S. *et al.* Distinct subclasses of medium spiny neurons differentially regulate striatal motor behaviors. *Proc. Natl. Acad. Sci.* **107**, 14845–14850 (2010).
7. Roseberry, T. K. *et al.* Cell-type-specific control of brainstem locomotor circuits by basal ganglia. *Cell* **164**, 526–537 (2016).
8. Sharples, S. A., Koblinger, K., Humphreys, J. M. & Whelan, P. J. Dopamine: a parallel pathway for the modulation of spinal locomotor networks. *Front. Neural Circuits* **8**, 55 (2014).
9. Jay, M., De Faveri, F. & McDearmid, J. R. Firing dynamics and modulatory actions of supraspinal dopaminergic neurons during zebrafish locomotor behavior. *Curr. Biol.* **25**, 435–444 (2015).
10. Dreyer, J. K., Herrik, K. F., Berg, R. W. & Hounsgaard, J. D. Influence of phasic and tonic dopamine release on receptor activation. *J. Neurosci.* **30**, 14273–14283 (2010).
11. Lambert, A. M. Dopaminergic control of locomotor patterning during development: a tail for the ages. *Front. Cell. Neurosci.* **10**, 95 (2016).
12. Clemens, S., Belin-Rauscent, A., Simmers, J. & Combes, D. Opposing modulatory effects of D1- and D2-like receptor activation on a spinal central pattern generator. *J. Neurophysiol.* **107**, 2250–2259 (2012).
13. Sharples, S. A. & Whelan, P. J. Modulation of rhythmic activity in mammalian spinal networks is dependent on excitability state. *eNeuro* **4**, 1–8 (2017).
14. Marder, E., O'Leary, T. & Shruti, S. Neuromodulation of circuits with variable parameters: single neurons and small circuits reveal principles of state-dependent and robust neuromodulation. *Annu. Rev. Neurosci.* **37**, 329–346 (2014).
15. Gutierrez, G. J., O'Leary, T. & Marder, E. Multiple mechanisms switch an electrically coupled, synaptically inhibited neuron between competing rhythmic oscillators. *Neuron* **77**, 845–858 (2013).
16. Bonnot, A., Morin, D. & Viala, D. Genesis of spontaneous rhythmic motor patterns in the lumbosacral spinal cord of neonate mouse. *Brain Res. Dev. Brain Res.* **108**, 89–99 (1998).
17. Dalrymple, A. N., Sharples, S. A., Osachoff, N., Lognon, A. P. & Whelan, P. J. A supervised machine learning approach to characterize spinal network function. *J. Neurophysiol.* **121**, 2001–2012 (2019).
18. Hanson, M. G. & Landmesser, L. T. Normal patterns of spontaneous activity are required for correct motor axon guidance and the expression of specific guidance molecules. *Neuron* **43**, 687–701 (2004).
19. Ren, J. & Greer, J. J. Ontogeny of rhythmic motor patterns generated in the embryonic rat spinal cord. *J. Neurophysiol.* **89**, 1187–1195 (2003).
20. Barriere, G., Mellen, N. & Cazalets, J.-R. Neuromodulation of the locomotor network by dopamine in the isolated spinal cord of newborn rat. *Eur. J. Neurosci.* **19**, 1325–1335 (2004).
21. Lapointe, N. P., Rouleau, P., Ung, R.-V. & Guertin, P. A. Specific role of dopamine D1 receptors in spinal network activation and rhythmic movement induction in vertebrates. *J. Physiol.* **587**, 1499–1511 (2009).
22. Picton, L. D., Nascimento, F., Broadhead, M. J., Sillar, K. T. & Miles, G. B. Sodium pumps mediate activity-dependent changes in mammalian motor networks. *J. Neurosci.* **37**, 906–921 (2017).
23. Acton, D., Broadhead, M. J. & Miles, G. B. Modulation of spinal motor networks by astrocyte-derived adenosine is dependent on D-like dopamine receptor signaling. *J. Neurophysiol.* **120**, 998–1009 (2018).
24. Mandadi, S. *et al.* Modulatory and plastic effects of kinins on spinal cord networks. *J. Physiol.* **594**, 1017–1036 (2016).
25. Gozal, E. A. *et al.* Anatomical and functional evidence for trace amines as unique modulators of locomotor function in the mammalian spinal cord. *Front. Neural Circuits* **8**, 134 (2014).
26. Milan, L., Barrière, G., De Deurwaerdère, P., Cazalets, J.-R. & Bertrand, S. S. Monoaminergic control of spinal locomotor networks in SOD1G93A newborn mice. *Front. Neural Circuits* **8**, 77 (2014).
27. Madriaga, M. A., McPhee, L. C., Chersa, T., Christie, K. J. & Whelan, P. J. Modulation of locomotor activity by multiple 5-HT and dopaminergic receptor subtypes in the neonatal mouse spinal cord. *J. Neurophysiol.* **92**, 1566–1576 (2004).
28. Gordon, I. T. & Whelan, P. J. Monoaminergic control of cauda-equina-evoked locomotion in the neonatal mouse spinal cord. *J. Neurophysiol.* **96**, 3122–3129 (2006).
29. Humphreys, J. M. & Whelan, P. J. Dopamine exerts activation-dependent modulation of spinal locomotor circuits in the neonatal mouse. *J. Neurophysiol.* **108**, 3370–3381 (2012).
30. Whelan, P., Bonnot, A. & O'Donovan, M. J. Properties of rhythmic activity generated by the isolated spinal cord of the neonatal mouse. *J. Neurophysiol.* **84**, 2821–2833 (2000).
31. Sharples, S. A. *et al.* Dopaminergic modulation of locomotor network activity in the neonatal mouse spinal cord. *J. Neurophysiol.* **113**, 2500–2510 (2015).
32. Zhu, H., Clemens, S., Sawchuk, M. & Hochman, S. Expression and distribution of all dopamine receptor subtypes (D(1)–D(5)) in the mouse lumbar spinal cord: a real-time polymerase chain reaction and non-autoradiographic in situ hybridization study. *Neuroscience* **149**, 885–897 (2007).
33. Jean-Xavier, C., Sharples, S. A., Mayr, K. A., Lognon, A. P. & Whelan, P. J. Retracing your footsteps: developmental insights to spinal network plasticity following injury. *J. Neurophysiol.* **119**, 521–536 (2018).
34. Hachoumi, L. & Sillar, K. T. Developmental stage-dependent switching in the neuromodulation of vertebrate locomotor central pattern generator networks. *Dev. Neurobiol.* https://doi.org/10.1002/dneu.22725 (2019).
35. Sharples, S. A., Burma, N. E., Leduc-Pessah, H., Jean-Xavier, C. & Whelan, P. J. Complex dopamine receptor interactions exert diverse modulation on spinal networks of the neonatal mouse. https://doi.org/10.13140/RG.2.2.17191.09125 (2017).
36. Sharples, S. A. & Whelan, P. J. Dopamine exerts concentration-dependent bidirectional modulation and evoked state-dependent NMDA-mediated rhythmicity in motor networks of the neonatal mouse spinal cord. https://doi.org/10.13140/RG.2.2.31925.27368 (2015).
37. LaHoste, G. J. & Marshall, J. F. The role of dopamine in the maintenance and breakdown of D1/D2 synergism. *Brain Res.* **611**, 108–116 (1993).
38. Rashid, A. J. *et al.* D1–D2 dopamine receptor heterooligomers with unique pharmacology are coupled to rapid activation of Gq/11 in the striatum. *Proc. Natl. Acad. Sci. U.S.A.* **104**, 654–659 (2007).
39. Thompson, J. L. *et al.* Age-dependent D1–D2 receptor coactivation in the lateral orbitofrontal cortex potentiates NMDA receptors and facilitates cognitive flexibility. *Cereb. Cortex* **26**, 4524–4539 (2016).
40. Lee, S. P. *et al.* Dopamine D1 and D2 receptor co-activation generates a novel phospholipase C-mediated calcium signal. *J. Biol. Chem.* **279**, 35671–35678 (2004).
41. Rashid, A. J., So, C. S., O'Dowd, B. F. & George, S. R. S. Heterooligomerization of D1 and D2 dopamine receptors in brain: implications for psychosis?. *Eur. Neuropsychopharmacol.* **16**, 193 (2006).
42. Falgairolle, M., Puhl, J. G., Pujala, A., Liu, W. & O'Donovan, M. J. Motoneurons regulate the central pattern generator during drug-induced locomotor-like activity in the neonatal mouse. *eLife* **6**, e26622 (2017).
43. Nascimento, F., Spindler, L. R. B. & Miles, G. B. Balanced cholinergic modulation of spinal locomotor circuits via M2 and M3 muscarinic receptors. *Sci. Rep.* **9**, 14051 (2019).
44. Smith, C. C. & Brownstone, R. M. Spinal motoneuron firing properties mature from rostral to caudal during post-natal development of the mouse. *BioRxiv* https://doi.org/10.1101/2020.05.15.097436 (2020).
45. Biswabharati, S. *et al.* Orexinergic modulation of spinal motor activity in the neonatal mouse spinal cord. *eNeuro* **5**, 1–20 (2018).

46. Quinlan, K. A., Schuster, J. E., Fu, R., Siddique, T. & Heckman, C. J. Altered postnatal maturation of electrical properties in spinal motoneurons in a mouse model of amyotrophic lateral sclerosis. *J. Physiol.* **589**, 2245–2260 (2011).
47. Button, D. C., Kalmar, J. M., Gardiner, K., Cahill, F. & Gardiner, P. F. Spike frequency adaptation of rat hindlimb motoneurons. *J. Appl. Physiol.* **102**, 1041–1050 (2007).
48. Bos, R. *et al.* Kv1.2 Channels promote nonlinear spiking motoneurons for powering up locomotion. *Cell Rep.* **22**, 3315–3327 (2018).
49. Miles, G. B., Dai, Y. & Brownstone, R. M. Mechanisms underlying the early phase of spike frequency adaptation in mouse spinal motoneurones. *J. Physiol.* **566**, 519–532 (2005).
50. Han, P., Nakanishi, S. T., Tran, M. A. & Whelan, P. J. Dopaminergic modulation of spinal neuronal excitability. *J. Neurosci.* **27**, 13192–13204 (2007).
51. Han, P. & Whelan, P. J. Modulation of AMPA currents by D(1)-like but not D(2)-like receptors in spinal motoneurons. *Neuroscience* **158**, 1699–1707 (2009).
52. Quinlan, K. A. & Kiehn, O. Segmental, synaptic actions of commissural interneurons in the mouse spinal cord. *J. Neurosci.* **27**, 6521–6530 (2007).
53. Butt, S. J. B. & Kiehn, O. Functional identification of interneurons responsible for left-right coordination of hindlimbs in mammals. *Neuron* **38**, 953–963 (2003).
54. Kiehn, O. & Butt, S. J. B. Physiological, anatomical and genetic identification of CPG neurons in the developing mammalian spinal cord. *Prog. Neurobiol.* **70**, 347–361 (2003).
55. Abbinanti, M. D., Zhong, G. & Harris-Warrick, R. M. Postnatal emergence of serotonin-induced plateau potentials in commissural interneurons of the mouse spinal cord. *J. Neurophysiol.* **108**, 2191–2202 (2012).
56. Zhong, G., Díaz-Ríos, M. & Harris-Warrick, R. M. Intrinsic and functional differences among commissural interneurons during fictive locomotion and serotonergic modulation in the neonatal mouse. *J. Neurosci.* **26**, 6509–6517 (2006).
57. Restrepo, C. E. *et al.* Transmitter-phenotypes of commissural interneurons in the lumbar spinal cord of newborn mice. *J. Comp. Neurol.* **517**, 177–192 (2009).
58. Butt, S. J. B., Harris-Warrick, R. M. & Kiehn, O. Firing properties of identified interneuron populations in the mammalian hindlimb central pattern generator. *J. Neurosci.* **22**, 9961–9971 (2002).
59. Zhang, Y. *et al.* V3 spinal neurons establish a robust and balanced locomotor rhythm during walking. *Neuron* **60**, 84–96 (2008).
60. Borowska, J. *et al.* Functional subpopulations of V3 interneurons in the mature mouse spinal cord. *J. Neurosci.* **33**, 18553–18565 (2013).
61. Borowska, J., Jones, C. T., Deska-Gauthier, D. & Zhang, Y. V3 interneuron subpopulations in the mouse spinal cord undergo distinctive postnatal maturation processes. *Neuroscience* **295**, 221–228 (2015).
62. Chopek, J. W., Nascimento, F., Beato, M., Brownstone, R. M. & Zhang, Y. Sub-populations of spinal v3 interneurons form focal modules of layered pre-motor microcircuits. *Cell Rep.* **25**, 146-156.e3 (2018).
63. Falgairolle, M. & O'Donovan, M. J. Feedback regulation of locomotion by motoneurons in the vertebrate spinal cord. *Curr. Opin. Physiol.* **8**, 50–55 (2019).
64. Grillner, S., Robertson, B. & Stephenson-Jones, M. The evolutionary origin of the vertebrate basal ganglia and its role in action selection. *J. Physiol.* **591**, 5425–5431 (2013).
65. Picton, L. D. & Sillar, K. T. Mechanisms underlying the endogenous dopaminergic inhibition of spinal locomotor circuit function in Xenopus tadpoles. *Sci. Rep.* **6**, 35749 (2016).
66. Beato, M. & Nistri, A. Serotonin-induced inhibition of locomotor rhythm of the rat isolated spinal cord is mediated by the 5–HT1 receptor class. *Proc. R. Soc. Lond. Ser. B Biol. Sci.* **265**, 2073–2080 (1998).
67. Sqalli-Houssaini, Y. & Cazalets, J.-R. Noradrenergic control of locomotor networks in the in vitro spinal cord of the neonatal rat. *Brain Res.* **852**, 100–109 (2000).
68. Bertuzzi, M. & Ampatzis, K. Spinal cholinergic interneurons differentially control motoneuron excitability and alter the locomotor network operational range. *Sci. Rep.* **8**, 1988 (2018).
69. Thirumalai, V. & Cline, H. T. Endogenous dopamine suppresses initiation of swimming in prefeeding zebrafish larvae. *J. Neurophysiol.* **100**, 1635–1648 (2008).
70. Murray, K. C. *et al.* Recovery of motoneuron and locomotor function after spinal cord injury depends on constitutive activity in 5-HT2C receptors. *Nat. Med.* **16**, 694–700 (2010).
71. Meng, D., Li, H.-Q., Deisseroth, K., Leutgeb, S. & Spitzer, N. C. Neuronal activity regulates neurotransmitter switching in the adult brain following light-induced stress. *Proc. Natl. Acad. Sci. U.S.A.* **115**, 5064–5071 (2018).
72. Ben-Ari, Y., Khazipov, R., Leinekugel, X., Caillard, O. & Gaiarsa, J. L. GABAA, NMDA and AMPA receptors: a developmentally regulated 'ménage à trois'. *Trends Neurosci.* **20**, 523–529 (1997).
73. Allene, C. & Cossart, R. Early NMDA receptor-driven waves of activity in the developing neocortex: physiological or pathological network oscillations?. *J. Physiol.* **588**, 83–91 (2010).
74. Koblinger, K. *et al.* Optogenetic activation of A11 region increases motor activity. *Front. Neural Circuits* **12**, 86 (2018).
75. Musienko, P. *et al.* Controlling specific locomotor behaviors through multidimensional monoaminergic modulation of spinal circuitries. *J. Neurosci.* **31**, 9264–9278 (2011).
76. Bolton, A. D. *et al.* A Diencephalic dopamine source provides input to the superior colliculus, where D1 and D2 receptors segregate to distinct functional zones. *Cell Rep.* **13**, 1003–1015 (2015).
77. Rotstein, H. G., Schneider, E. & Szczupak, L. Feedback signal from motoneurons influences a rhythmic pattern generator. *J. Neurosci.* **37**, 9149–9159 (2017).
78. Matsunaga, T., Kohsaka, H. & Nose, A. Gap junction-mediated signaling from motor neurons regulates motor generation in the central circuits of larval. *J. Neurosci.* **37**, 2045–2060 (2017).
79. Marder, E. & Bucher, D. Central pattern generators and the control of rhythmic movements. *Curr. Biol.* **11**, R986–R996 (2001).
80. Song, J., Ampatzis, K., Rebecka Björnfors, E. & El-Manira, A. Motor neurons control locomotor circuit function retrogradely via gap junctions. *Nature* **529**, 399–402 (2016).
81. Pujala, A., Blivis, D. & O'Donovan, M. J. Interactions between dorsal and ventral root stimulation on the generation of locomotor-like activity in the neonatal mouse spinal cord. *eNeuro* **3**, 1–16 (2016).
82. Bhumbra, G. S. & Beato, M. Recurrent excitation between motoneurones propagates across segments and is purely glutamatergic. *PLoS Biol.* **16**, e2003586 (2018).
83. Danner, S. M. *et al.* Spinal V3 interneurons and left-right coordination in mammalian locomotion. *Front. Cell. Neurosci.* https://doi.org/10.3389/fncel.2019.00516 (2019).
84. Rivera-Oliver, M. *et al.* Adenosine A-dopamine d receptor heteromers control the excitability of the spinal motoneuron. *Mol. Neurobiol.* **56**, 797–811 (2019).
85. Acevedo, J. *et al.* Caffeine stimulates locomotor activity in the mammalian spinal cord via adenosine A1 receptor-dopamine D1 receptor interaction and PKA-dependent mechanisms. *Neuropharmacology* **101**, 490–505 (2016).
86. Kiehn, O. Decoding the organization of spinal circuits that control locomotion. *Nat. Rev. Neurosci.* **17**, 224–238 (2016).
87. Dougherty, K. J. *et al.* Locomotor rhythm generation linked to the output of spinal shox2 excitatory interneurons. *Neuron* **80**, 920–933 (2013).

88. Caldeira, V., Dougherty, K. J., Borgius, L. & Kiehn, O. Spinal Hb9::cre-derived excitatory interneurons contribute to rhythm generation in the mouse. *Sci. Rep.* **7**, 41369 (2017).
89. Perreault, M. L. *et al.* The dopamine D1–D2 receptor heteromer localizes in dynorphin/enkephalin neurons: increased high affinity state following amphetamine and in schizophrenia. *J. Biol. Chem.* **285**, 36625–36634 (2010).
90. Clemens, S. & Hochman, S. Conversion of the modulatory actions of dopamine on spinal reflexes from depression to facilitation in D3 receptor knock-out mice. *J. Neurosci.* **24**, 11337–11345 (2004).
91. Vinay, L., Brocard, F. & Clarac, F. Differential maturation of motoneurons innervating ankle flexor and extensor muscles in the neonatal rat. *Eur. J. Neurosci.* **12**, 4562–4566 (2000).
92. Nakanishi, S. T. & Whelan, P. J. Diversification of intrinsic motoneuron electrical properties during normal development and botulinum toxin-induced muscle paralysis in early postnatal mice. *J. Neurophysiol.* **103**, 2833–2845 (2010).
93. Durand, J. *et al.* Developing electrical properties of postnatal mouse lumbar motoneurons. *Front. Cell. Neurosci.* **9**, 349 (2015).
94. Ha, N. T. & Dougherty, K. J. Spinal Shox2 interneuron interconnectivity related to function and development. *Elife* **7**, e42519 (2018).
95. Husch, A., Dietz, S. B., Hong, D. N. & Harris-Warrick, R. M. Adult spinal V2a interneurons show increased excitability and serotonin-dependent bistability. *J. Neurophysiol.* **113**, 1124–1134 (2015).
96. Jean-Xavier, C., Mentis, G. Z., O'Donovan, M. J., Cattaert, D. & Vinay, L. Dual personality of GABA/glycine-mediated depolarizations in immature spinal cord. *Proc. Natl. Acad. Sci. U.S.A.* **104**, 11477–11482 (2007).
97. Jha, U. & Thirumalai, V. Neuromodulatory selection of motor neuron recruitment patterns in a visuomotor behavior increases speed. *Curr. Biol.* **30**, 788-801.e3 (2020).
98. Reimer, M. M. *et al.* Dopamine from the brain promotes spinal motor neuron generation during development and adult regeneration. *Dev. Cell* **25**, 478–491 (2013).
99. Lambert, A. M., Bonkowsky, J. L. & Masino, M. A. The conserved dopaminergic diencephalospinal tract mediates vertebrate locomotor development in zebrafish larvae. *J. Neurosci.* **32**, 13488–13500 (2012).
100. Pflieger, J.-F., Clarac, F. & Vinay, L. Postural modifications and neuronal excitability changes induced by a short-term serotonin depletion during neonatal development in the rat. *J. Neurosci.* **22**, 5108–5117 (2002).
101. Gackière, F. & Vinay, L. Serotonergic modulation of post-synaptic inhibition and locomotor alternating pattern in the spinal cord. *Front. Neural Circuits* **8**, 102 (2014).
102. Commissiong, J. W. The development of catecholaminergic nerves in the spinal cord of rat. II. Regional development. *Brain Res.* **313**, 75–92 (1983).
103. Kelly, E., Jenner, P. & Marsden, C. D. Evidence that [3H]dopamine is taken up and released from nondopaminergic nerve terminals in the rat substantia nigra in vitro. *J. Neurochem.* **45**, 137–144 (1985).
104. Hoyer, D., Waeber, C., Schoeffter, P., Palacios, J. M. & Dravid, A. 5-HT1C receptor-mediated stimulation of inositol phosphate production in pig choroid plexus. A pharmacological characterization. *Naunyn. Schmiedebergs Arch. Pharmacol.* **339**, 252–258 (1989).
105. Hoyer, D. & Karpf, A. [125I]SCH 23982, a 'selective' D-1 receptor antagonist, labels with high affinity 5-HT1C sites in pig choroid plexus. *Eur. J. Pharmacol.* **150**, 181–184 (1988).
106. Lanteri, C., Salomon, L., Torrens, Y., Glowinski, J. & Tassin, J.-P. Drugs of abuse specifically sensitize noradrenergic and serotonergic neurons via a non-dopaminergic mechanism. *Neuropsychopharmacology* **33**, 1724–1734 (2008).
107. Bischoff, S. *et al.* Interaction of the D1 receptor antagonist SCH 23390 with the central 5-HT system: radioligand binding studies, measurements of biochemical parameters and effects on L-5-HTP syndrome. *J. Recept. Res.* **8**, 107–120 (1988).
108. Parent, M. B., Habib, M. K. & Baker, G. B. Time-dependent changes in brain monoamine oxidase activity and in brain levels of monoamines and amino acids following acute administration of the antidepressant/antipanic drug phenelzine. *Biochem. Pharmacol.* **59**, 1253–1263 (2000).
109. Mor, Y. & Lev-Tov, A. Analysis of rhythmic patterns produced by spinal neural networks. *J. Neurophysiol.* **98**, 2807–2817 (2007).

Acknowledgments

We would like to acknowledge support from the Whelan Lab and technical support from Dr. Heather Leduc-Pessah and Rebecca Dalgarno on immunoprecipitation experiments and Gail Rauw on HPLC experiments. Spinalcore software was a kind gift from Prof A. Lev-Tov (Hebrew University).

Author contributions

S.A.S. performed and analyzed whole-cell and network electrophysiology, N.E.B., performed and analyzed CoIP, J.B.F. performed recordings from V3 interneurons, G.B.B. performed and analyzed HPLC, and S.A.S., C.H.T.K. and S.E.A.E. performed IHC and imaging experiments. S.A.S., C.J.-X. and P.J.W. interpreted results. S.A.S. prepared figures and drafted the manuscript. T.T., Y.Z. and P.J.W. contributed to experimental design and procured funding. S.A.S., C.J.-X. and P.J.W. conceived and designed the research, and edited the manuscript. All authors reviewed and approved the final version of the manuscript.

Funding

We acknowledge studentships from the Natural Sciences and Engineering Research Council of Canada (NSERC-PGS-D: SAS), the Canadian Institute for Health Research (CIHR: NEB), Alberta Innovates—Health Solutions (AIHS: SAS, NEB), Hotchkiss Brain Institute (SAS, NEB) and the Faculty of Veterinary Medicine (CHTK). This research was supported by grants from NSERC (Discovery grant: PJW), CIHR (PJW, YZ) and the VP Research Office and the Faculty of Medicine & Dentistry at the University of Alberta (GBB).

Competing interests

The authors declare no competing interests.

Additional information

Supplementary information is available for this paper at https://doi.org/10.1038/s41598-020-73230-w.

Correspondence and requests for materials should be addressed to P.J.W.

Reprints and permissions information is available at www.nature.com/reprints.